The University of Calgary

A Continuous Automated
Dielectrophoretic System

by

Richard J. Adamson

A THESIS

SUBMITTED TO THE FACULTY OF GRADUATE STUDIES

IN PARTIAL FULFILLMENT OF THE REQUIREMENTS FOR THE

DEGREE OF MASTER OF SCIENCE

DEPARTMENT OF ELECTRICAL ENGINEERING

CALGARY, ALBERTA

April, 1986

THE UNIVERSITY OF CALGARY

FACULTY OF GRADUATE STUDIES
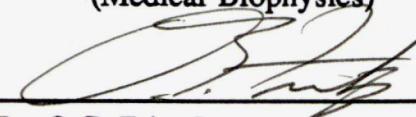
The undersigned certify that they have read, and recommend to the Faculty of
Graduate Studies for acceptance, a thesis entitled "A Continuous Automated Dielectro-
phoretic System" submitted by Richard J. Adamson in partial fulfillment of the require-
ments for the degree of Master of Science.

Supervisor, Dr. K.V.I.S. Kaler
(Electrical Engineering)

Dr. J. Beck
(Medical Biophysics)

Dr. O.G. Fritz Jr.
(Physics)

Dr. R.H. Johnson
(Electrical Engineering)

date 6 May 1986.

ABSTRACT

Dielectrophoresis has been shown to be potentially useful as a technique for identifying dielectric (polarisation) properties of particles and separating them on that basis. Particles range from polystyrene microspheres to complex biological cells.

An automated system is described which allows the characterisation and, potentially, separation of cell species on a continuous basis, based on their dielectric spectra. Here a narrow sample stream suspended within a larger sheath is injected between a pair of *isomotive* electrodes (for which the force on the particles is independent of position). Upon application of an AC field the sample particles undergo positive or negative displacement depending on their polarisation characteristics relative to the medium. Deflection is monitored by a 1024 element photo-diode array which detects the light of a *HeNe* laser scattered by the sample particles. Response may be measured from low frequencies up to 50 MHz under computer control. This enables the dielectrophoretic spectra to be obtained with minimum human intervention.

Details of the design and preliminary test results, based on yeast cells (*S. cerevesiae*) and polystyrene-DVB microspheres are presented.

ACKNOWLEDGEMENTS

DEDICATION

This thesis is dedicated to the memory of my step-father, Neil Victor German, always remembered for his high standards and unyielding integrity, who generously provided me with a loving environment, unceasing support, and encouragement to go on.

TABLE of CONTENTS

LIST of TABLES

LIST of FIGURES

LIST of SYMBOLS

Operators:

∇ .... gradient operator

$| \cdots |$ .... magnitude

$Re\left\{ \cdots \right\}$ .... real part

Symbols:

α, β, γ .... three major dispersions observed in biological

                                      systems(cells, tissue samples)

α .... polarisability

α_{eH} .... electronic polarisability of hydrogen

ϕ .... energy barrier

ε' .... real component of the permittivity

ε'' .... imaginary component of the permittivity

                                      (dielectric loss)

ε_0 .... permittivity of free space

$\varepsilon_1, \varepsilon_2$ .... relative permittivities of fluid and particle

$\varepsilon_1, \varepsilon_2$ .... relative permittivities of a bilayer capacitor

$\varepsilon_1^*, \varepsilon_2^*$ .... complex permittivities of fluid and particles

$\hat{\varepsilon}_1^*$ .... complex conjugate of ε_1^*

$\Delta\varepsilon_{bl}$ .... dielectric increment due to bound

xii

M .... diffuse counterion adjustment factor

n .... free charge carrier concentration

$\vec{P}$ .... electric dipole moment per unit volume

q .... charge

q_e .... electronic charge

(r, θ, z) .... cylindrical coordinate parameters

r_{60} .... scaling factor for isomotive electrodes

s .... standard deviation

T .... absolute temperature (Kelvin)

u_b .... mechanical mobility of bound counterions

u_0 .... solution mobility of counterions

V .... voltage (peak to peak magnitude)

$V(t)$ .... time varying voltage

v_2 .... volume concentration of particles

z .... see (r, θ, z)

CHAPTER 1

INTRODUCTION TO SEPARATION METHODS

In the life sciences there is an obvious requirement for both separation of cells of different species and of subpopulations within the species which differ in ways such as growth rate, size, surface properties, and other characteristics.

A system is presented here which may be used to characterise and physically separate cells in a continuous fashion using the principles of **dielectrophoresis (DEP)** [1]. DEP is the motion (*phoresis*) of neutral, polarisable particles due to non-uniform field effects.

In the past numerous cell characterisation or separation techniques have been devised and used to varying extents in the biological sciences; however, each has been applicable in a limited set of circumstances. In addition, many of these techniques have side effects which may cause artifacts in further analysis. It is appropriate at this point to briefly discuss the most common approaches and their associated areas of application and limitations.

1.1. Isopycnic Density Gradient Centrifugation

In the isopycnic density gradient technique cells are centrifuged while suspended in a medium of spatially varying density which results in their localisation in a region at which their own average density equals that of the local medium [2,3]. This technique is of practical interest when the cells to be

separated have a much different density from all others in the sample. The requirements on the media used for this technique are strict as the cells must not clump (aglutinate) nor should the media cause the cells to change density from osmolality or media absorption effects. In addition to these restrictions the mechanical properties of the media, such as low viscosity and appropriate density range (1.0 to 1.3)[2] must be suitably selected to achieve good separation.

1.2. Centrifugal Elutriation

When the densities do not vary widely but the size of the desired cells differ from others in the suspension, a variation of this technique, known as centrifugal elutriation, may be used in which centrifugal sedimentation takes place against a medium counterflow [4,5]. The cells are then recovered in order of sedimentation velocity. This technique shares most of the difficulties of isopycnic density gradient centrifugation regarding media requirements though extraction of various fractions of the sample is simplified.

1.3. Electrophoresis

Most cell types maintain a net negative charge at physiological pH [2]. Thus when placed in an electrostatic field, they tend to translate toward the anode. Electrophoresis exploits this property by combining it with the density gradient technique mentioned earlier. The cells here are separated according to "electrophoretic mobility". This term includes the effects of cell density,

surface charge, and other parameters. The various subpopulations are extracted according to their locations within the gel. This technique suffers from additional restrictions over those imposed in other density gradient techniques, in that ionic concentration must be minimised to reduce thermally generated convective mixing [2,6,7,8]. To meet the osmolality restrictions, however, an alternative buffer must be used (e.g. sucrose, glucose, sorbitol, or glycine). Unfortunately these promote cell aglutination.

1.4. Free-flow Electrophoresis

Free-flow electrophoresis[9] is a variation of this previous technique to allow continuous, as opposed to batch separation to occur. In this technique a stream of medium flows between two electrodes and the sample stream is injected near the cathode. By the time the flow has passed the electrode section of the separation cell the subpopulations are distributed perpendicular to the flow direction according to their electrophoretic mobilities. It is then a matter of splitting the flow to obtain the cell population of interest. The difficulties experienced with this technique are similar in nature to batch electrophoresis.

1.5. Phase Partitioning

In phase partitioning the cell sample is suspended in an aqueous solution with two or more immiscible polymers of differing properties [10,2]. The cells collect preferentially within one of the phases and are then separated out

with that phase. The collection criteria include electrostatic potential, hydrophobic properties, or ligand affinity, depending on the constituents of each polymer phase. Major difficulties with this technique are the lack of generality and the requirement of multiple partitioning in most cases.

1.6. Magnetic Properties

Separation may be achieved using magnetic phenomena, though this is less common. Two approaches have been taken. One takes advantage of the high permeability of the iron component of haemoglobin and has been used to separate malaria infected red blood cells from whole blood [2,4]. The other approach involves coating magnetic particles with a ligand and then passing the resulting suspension through an intense magnetic field.

1.7. Surface Properties

Surface properties may be used in a variety of ways for cell separation. Passing a cell suspension over a substrate to which a given cell subpopulation tends to adhere (e.g. nylon, rayon, cotton, glass wool fibres, or beads of other polymers) is a direct technique [2]. However the eventual requirement of cell removal from these substrates, often requiring use of enzymes or chelating agents, restricts this technique primarily to negative selection applications.

In aglutination techniques the cell sample is exposed to an aglutinin causing a subpopulation to clump then sediment. This can be successful in specific circumstances, and recovery is straight forward (exposure to inhibitory sugars

will reverse the aglutination), however the limited selection of aglutinins prevents broad application [2].

Cell affinity chromatography[2, 11] is similar to adherence separation; however substrates are first coated with a receptor to which the required cells will bind.

In addition to these surface techniques there are numerous variations, such as lysis by antibody (e.g. monoclonal antibody techniques) causing alteration of surface charge characteristics, which may be followed by electrophoresis [2].

1.8. Flow Cytometry

Of all the proven techniques flow cytometry is probably the most flexible [2, 12]. This encompasses several of other analysis technologies. The system consists of two main portions: the first being responsible for identification of the required subpopulation, and the second for separation.

The stream is broken by ultrasonic vibration into tiny droplets containing at most one particle. The identification stage may then select particles either by size (light scattering) or on the basis of fluorescence (which requires previous treatment of the sample with a fluorescent tag of appropriate specificity) or both in order to obtain two dimensional correlations.

The particles are then made to pass between a pair of electrodes. The polarity of the electric field is determined by an electronic signal from the previous identification stage. The cells are then sorted by the resulting

electrostatic deflection.

1.9. Dielectrophoresis

Dielectrophoresis (DEP) is the motion of neutral particles resulting from electric field nonuniformities [1]. Unlike electrophoresis it does not require a net charge on the particle in motion and is independent of field polarity. Here the force acting on the neutral particle is a function of the dielectric properties of the particle with respect to the surrounding medium, the local field magnitude and gradient, and the particle shape and volume (see Equation 3.2 and Figure 3.1). This means that, because there are no requirements of binding of receptors, or substrate adherence, the cells undergoing DEP may potentially be further analysed by other techniques without the introduction of artifacts. Each cell species has a different DEP spectrum which varies with numerous biological changes (both natural and artificially induced) [1,13]. Thus the DEP "fingerprinting" technique is potentially much more widely applicable than others.

1.10. The Continuous Automated DEP System

Early work on a continuous DEP system indicates that this may be successfully applied for biological systems [14,1]. The following work describes the implementation of an automated continuous DEP system in which several refinements have been made. An isomotive electrode pair has been obtained using numerically controlled machining techniques, a wet electrode

configuration has been chosen to allow measurements at lower frequencies than the earlier continuous systems permitted, and the signal source and data acquisition systems have been interfaced to a microcomputer system for automated control.

Chapter 2 provides a review of past literature on dielectrophoresis as it has been applied to biological systems. This is followed, in Chapter 3, by a brief summary of the more relevant theory required to understand the operation of the DEP system. Chapter 4 consists of conceptual and detailed descriptions of the instrument. Results of characterisation of the system and DEP spectra for *Saccharomyces cerevisiae* and divinylbenzene (DVB) microspheres are detailed in Chapter 5. Chapter 6 includes conclusions and suggests possible directions for further work.

CHAPTER 2

DIELECTROPHORESIS of BIOLOGICAL CELLS

Dielectrophoresis has primarily been applied to biological cells in two ways. First, as a method of measurement, it has been used to obtain the polarisation spectrum over a wide range of applied field frequencies, and second for separation of cells of differing polarisation characteristics.

An early observation was that fat particles would aggregate into strings when exposed to near-uniform AC fields (see Pohl[1] Chapter 15 for a good overview). This was an example of mutual dielectrophoresis or pearl chain formation (see Chapter 3). The effect was subsequently observed for red blood cells, and various unicellular organisms [15]. The frequency selective orientation of oblong cells was also observed [15, 1].

Pohl and Hawk[16] first successfully collected yeast cells using a pin-plate electrode geometry and subsequently "yield spectra" (collection rate at electrode surfaces *vs.* frequency) were obtained. These spectra were compared for cells of varying age, and treatment (such as exposure to heat, chemical agents, and ultraviolet radiation) [1]. All of these parameters showed a marked influence on the collection spectra and therefore on the effective polarisability of the cells. Comparison studies of hemophilic dog platelets[1] showed a stronger collection peak at approximately 1 *MHz* for hemophilic male platelets

than for those of a normal dog. Other studies have been done on red cells, chloroplasts, mitochondria, and many varieties of bacteria [1, 15].

Zimmerman [17] has used the pearl chain effect to collect cells before applying strong pulsed fields to cause fusion, creating giant multinucleated cells. Chen and Pohl[18] obtained DEP spectra for yeast cells using a single cell levitation system. This technique involved recording the voltage at which a cell would release from the upper electrode of a wire-wire system. A more recent single-cell levitation study has been performed by Kaler and Pohl[19] using a pin-ring geometry in which similar results were obtained for yeast as well as a spectrum for *Netrium digitus* .

Mason and Townsley[20] used a continuous flow system to separate live yeast cells (*S. cerivisiae* var. *ellipsoidus*) from dead (autoclaved) achieving separation efficiencies as high as 75%. This system relied on a simple cylindrical geometry in which the cells with higher permittivity collected about the central wire electrode and settled out through a narrow aperture surrounding it at the bottom of the chamber [1]. This type of electrode geometry is far from optimal due to cells which start out in the region near the outer electrode due to the extremely position dependent nature of the DEP force (see Chapter 3).

Pohl achieved positive and negative DEP using a half-isomotive chamber [1]. Later Pohl, Kaler, and Pollock[14] developed a system which allowed positive and negative DEP in a continuous system using a nearly isomotive electrode chamber, however separation was not performed at that time.

A characterisation technique recently developed at the University of Calgary uses laser doppler velocimetry to obtain statistical information about particle velocities within a small volume of sample undergoing dielectrophoresis [21]. Measurements have been performed using the same isomotive electrode geometries as are used in the current work, as well as other geometries, with some success. This allows precise and immediate measurement of dielectrophoresis, resulting from direct velocity measurement, and does not require restriction of the sample into a narrow stream because particles outside of a small selected volume within the sample chamber are ignored. This technique offers greatly improved measurement technology without directly contributing to that of separation systems.

Much study has been made of the dielectric properties of biological materials in suspension, homogenised, as intact tissue samples, and *in situ*. There are numerous reviews of this work ([22, 23, 24] for example).

These measurements are all based on the change in impedance of a chamber over a range of frequencies, when filled with sample. The high concentrations of particles required for these measurements result in particle-particle interaction effects. In addition to this, at low frequency, conductivity effects so dominate that the test equipment must be extremely sensitive to measure the relatively small reactive component [24]. Electrode polarisation effects, due to the charge layer at the boundary between electrodes and solution may produce erroneous readings. At high frequencies, transmission-line

approaches are taken, in which the sample is the dielectric material in the transmission line and measurements are made of the response of the line, either in time domain or in the frequency domain, to determine the loss and permittivity associated with the sample.

In general, for biological systems, the permittivity changes in three regions of the spectrum. These are labelled, in order of increasing field frequency, as the α, β, and γ *dispersions* [22,23]. (See Figure 2.1 for a typical spectrum.)

The main advantage of DEP over these other measurement techniques is that in all cases the capacitive approach measures the bulk effects averaged over the volume including medium and sample, in the case of DEP. However, the effective polarisability obtained is due to the individual particles and their interaction with the local medium.

For this reason suspensions of extremely low sample volumetric concentration may be used to obtain reliable measurements. In addition much smaller samples may be used (as little as 250 μl to obtain twelve points in a spectrum with the system described here).
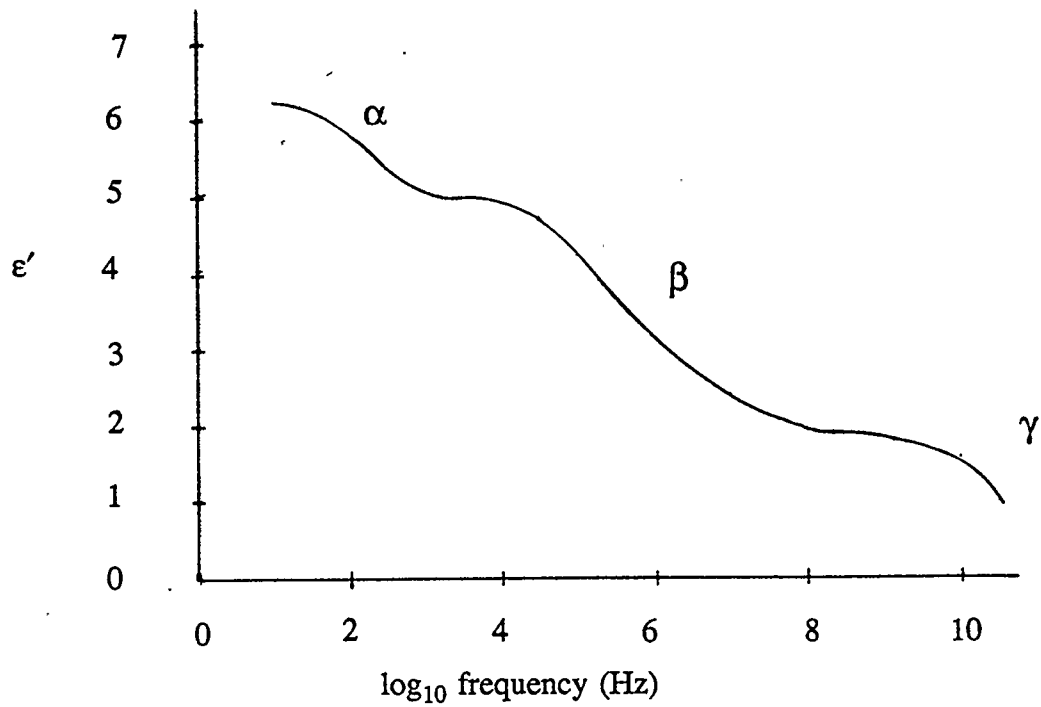
Figure 2.1:

Approximate permittivity spectrum for muscle tissue with three major dispersions marked α, β, and γ (after Schwan[22]).

The following applies to Figure 3.1.

CHAPTER 3

THEORY

3.1. Dielectrophoresis

Consider a charged body influenced by an externally applied uniform electric field (Figure 3.1 a). An electrostatic force will be directed toward the electrode of opposite polarity to that of the charge on the body.

If the body is *neutral* (equal positive and negative charge) then there will be a finite charge separation within the body due to the applied field. This separation, or *polarisation* may be represented by a point *dipole* of *moment* $\vec{\mu}$ of magnitude $| \vec{\mu} | = (q \cdot d)$ where q is the total charge of one polarity, and d is the distance between charge centres of opposite sign.

The units of dipole moment are the Debye (D). If two charges equal in magnitude to that of the electron, one positive and one negative, are held 2.38 *nm* apart then $\vec{\mu} = 1$ *D*, or, in SI units, 3.33×10^{-30} *C m*.

The polarisation is a result of electrostatic forces on the charges, similar to that described for the charged body case, above, drawing the charges of each sign in opposing directions. Forces may thus be pictured acting on each end of the dipole in opposite directions and of equal magnitude. In the uniform-field case the resultant force is zero (Figure 3.1 a). However, if the applied field is non-uniform then there will be a net force acting on the particle in the direction
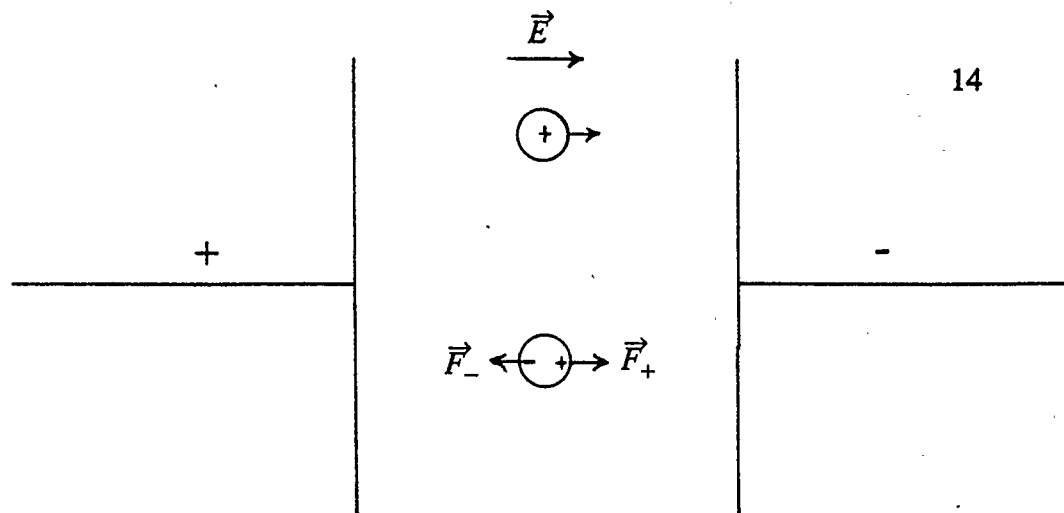
(a)
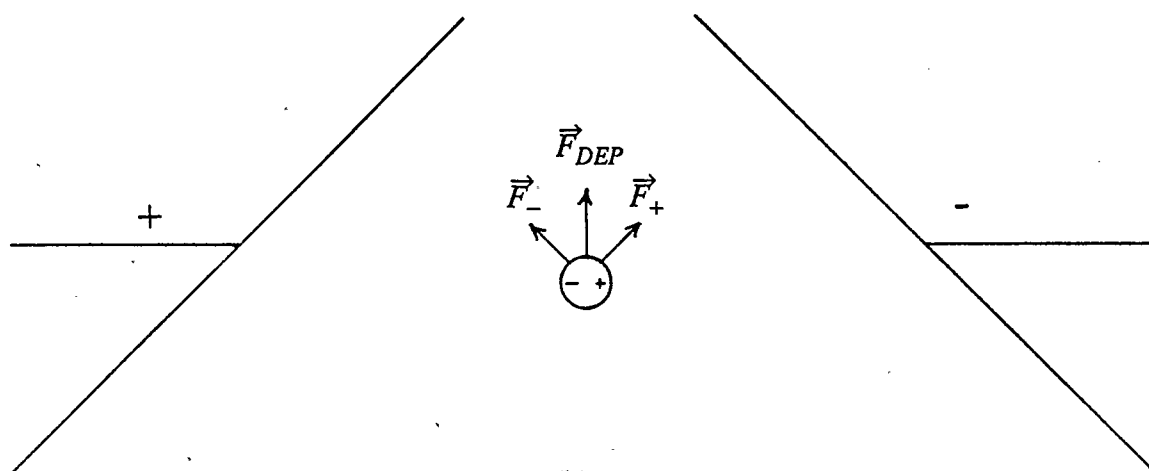
(b)

Figure 3.1:

(a) uniform field: net force on charged body - none on polarised body.

(b) non-uniform field: net force on polarised body parallel to field gradient, independent of field direction, thus AC field may be used.

of the field gradient (Figure 3.1 b). The motion of a particle acted on by this force is called *dielectrophoresis* [1].

The extent to which a particle will polarise for a given field strength is called the *polarisability*

$$\alpha = \frac{|\vec{\mu}|}{|\vec{E}|} \quad . \tag{3.1}$$

In general a particle of finite polarisability in a nonuniform field may be modelled as containing dipole, quadrupole, octupole, *et cetera* moments. Adamson and Kaler [25] have shown that the dipole term completely dominates for the field geometry used here. Using this assumption the force exerted on a spherical 'ideal' dielectric particle may be described by[1]

$$\vec{F}_d = 2\pi a^3 \, \varepsilon_0 \left[\varepsilon_1 \frac{\varepsilon_2 - \varepsilon_1}{\varepsilon_2 + 2\varepsilon_1} \right] \nabla |\vec{E}|^2 \quad . \tag{3.2}$$

Here the particle radius is a and permittivity ε_2, suspended in an ideal dielectric medium of permittivity ε_1 where $\vec{E}$ is the electric field vector.

As may be seen in Equation 3.2 magnitude of the force is dependent on the electric field magnitude but not the field direction, thus AC fields may be used. In addition the sign of the force is fixed by the difference between the two permittivities ($\varepsilon_1 - \varepsilon_2$), thus, if the medium has a higher permittivity than the particle, the net force will be directed down the field gradient. This latter effect is termed *negative dielectrophoresis* [1].

When a dipole is inserted into an electric field the net field in the vicinity of the dipole will be disturbed in exactly the same way as for a dielectric particle of identical dipole moment inserted at the same point (Figure 3.2a). If a second dielectric particle is placed within this local field gradient DEP will take place attracting the two particles together or forcing them apart (Figure 3.2b). This is called *mutual dielectrophoresis* and, if the force is attractive, results in the formation of strings of particles parallel to the field lines known as *pearl chains*[1] (see Figure 3.3).

When an AC field is applied to a material the current through the material will lead the voltage across it by some finite time. When the material is conduction dominated the lead approaches 0°, if the material is permittivity dominated (nearly an ideal dielectric) the lead approaches 90°. Any real material will fall between these extremes and it is therefore convenient to speak of a single parameter which takes into account both permittivity and loss effects. In this case it is more appropriate to talk about a complex permittivity (ε^*), where

$$\varepsilon^* = \varepsilon' - j\varepsilon'' \tag{3.3}$$

where ε' is the real component of the permittivity and ε'' takes into account all energy loss mechanisms including conduction losses.

The effective force ($\vec{F}_{eff}$) on the particle is

$$\vec{F}_{eff} = \vec{\mu}_{eff} \cdot \nabla \vec{E}_0 \tag{3.4}$$

where $\vec{\mu}_{eff}$ is the effective dipole moment of the particle. For linear dielectrics $\vec{\mu}_{eff}$ is collinear (either parallel or antiparallel) with $\vec{E}_0$ [26]. Thus Pohl [1]

(a)

(b)
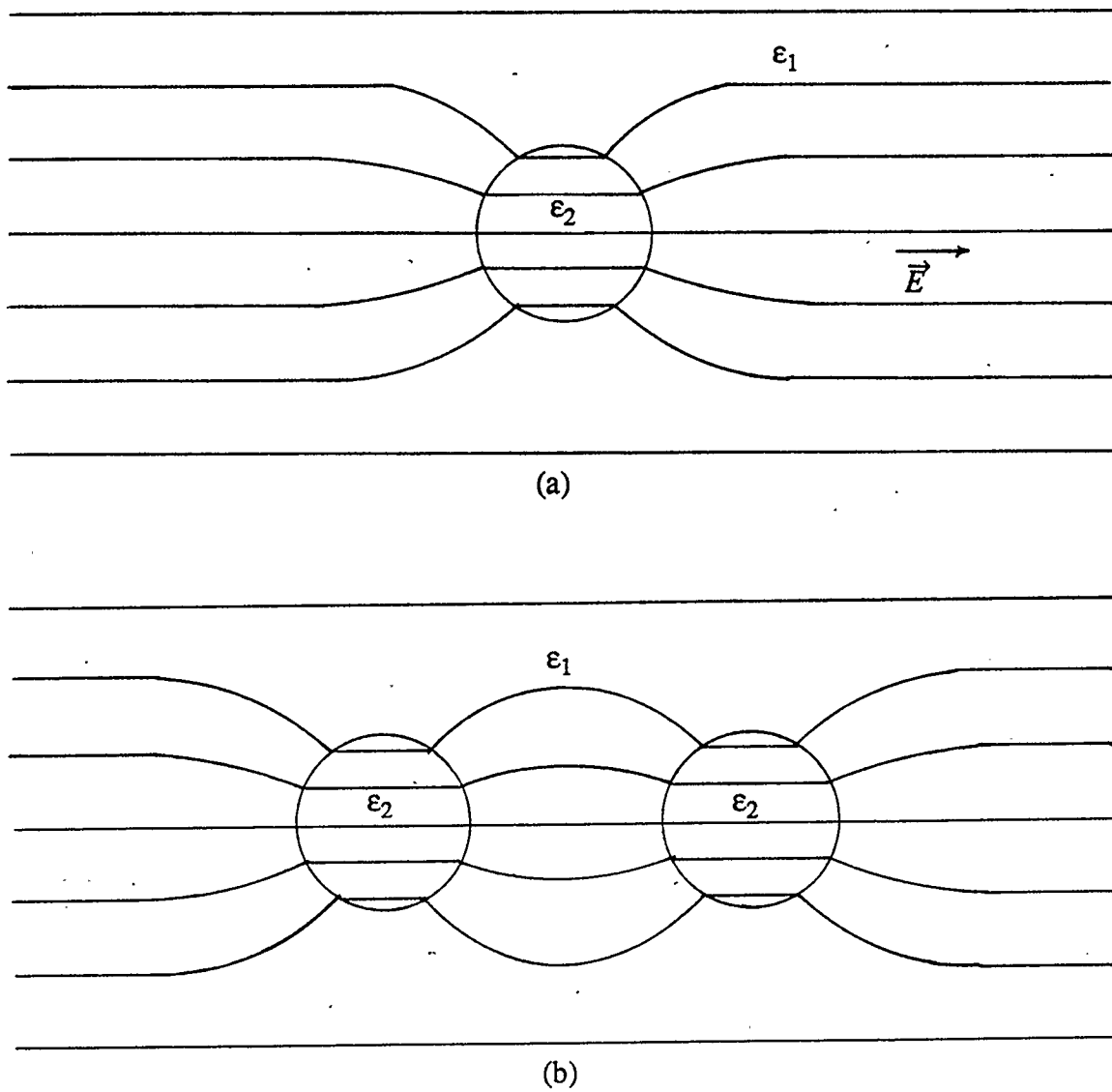
Figure 3.2:

(a) Uniform field distorted by polarised particle ($\varepsilon_2 > \varepsilon_1$)

(b) local field gradient in region of polarised particles results in mutual attraction (DEP).
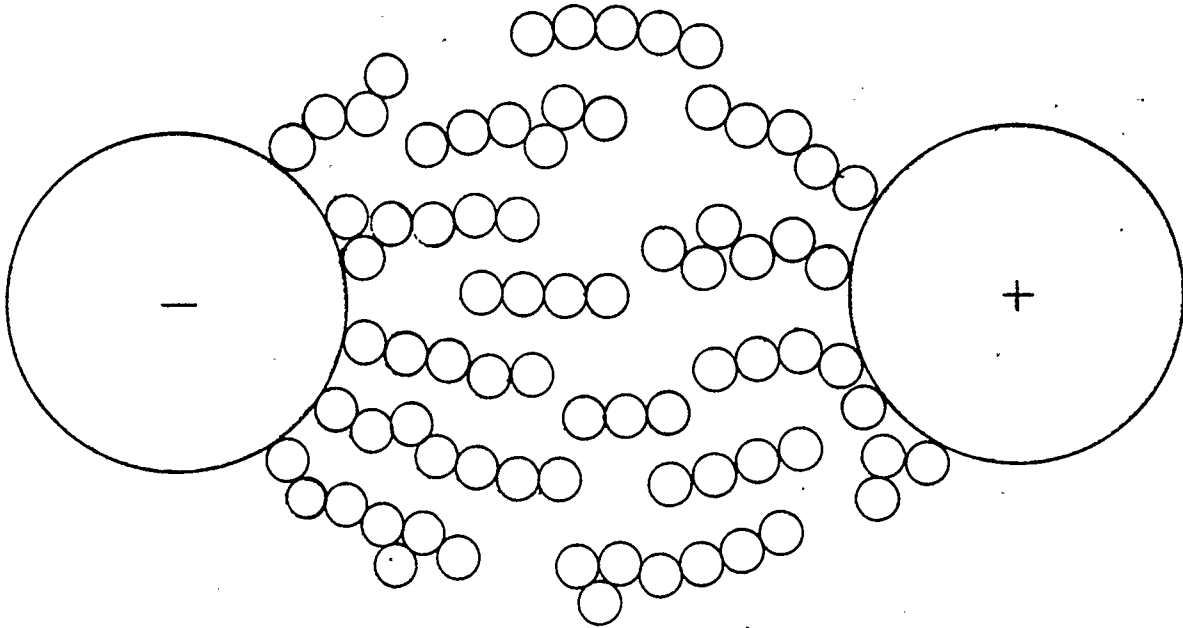
Figure 3.3:

Mutual DEP causes formation of *pearl chains* parallel to the electric field
lines for $\varepsilon_2 > \varepsilon_1$ (pin-pin electrode geometry illustrated here).

finds the force in the lossy dielectric case to be

$$\vec{F} = 2\pi a^3 \, \varepsilon_0 \, \mathrm{Re}\left\{\varepsilon_1^* \, \frac{(\varepsilon_2^* - \varepsilon_1^*)}{(\varepsilon_2^* + 2\varepsilon_1^*)}\right\} \nabla|\vec{E}|^2 \qquad (3.5)$$

where ε_1^* is the complex conjugate of ε_1^*; ε_1^* and ε_2^* refer to the complex permittivities of the medium and particle respectively, and the Re{ } operator refers to the real part of the function in braces. The real part is required in order to meet the requirement of $\vec{\mathrm{p}}_{eff}$ collinear with $\vec{E}_0$. (There is some question about the validity of the derivation of Equation 3.5. Jones and Kallio[26] present an alternative approach.)

For simplicity (3.5) is often stated as

$$\vec{F}_d = 2\pi a^3 \, \varepsilon_0 \, K_e \, \nabla|\vec{E}|^2 \qquad (3.6)$$

wherein the factor K_e represents the *effective polarisability* of the particle in the medium.

The $\nabla|\vec{E}|^2$ dependence of the force equation results in extremely position dependent forces for many easily achieved electrode geometries [27]. In such cases the force varies with position as n^{th} power of particle position:

$$\vec{F} = k \, r^n \qquad (3.7)$$

when using a system of cylindrical coordinates (r, θ, z) with the origin at the central electrode. For example, it was shown that, for spherical and cylindrical geometries $n = -5$ and $n = -3$ respectively [27].

For the purposes of material characterisation using DEP it is desirable to obtain a field geometry which minimises the position dependence of the force on particles ($n = 0$). It has thus been found[27] that electrodes of the form

$$r = r_{60} \sin(3/2 \, \theta \,)^{-2/3} \tag{3.8}$$

will provide the required field geometry (Figure 3.4). This is referred to as an *isomotive* electrode geometry. The force equation, solving Equation (3.6) for isopotential lines described by (3.8) yields

$$F_d = \frac{9}{2} \, \pi a^2 \, V^2 \, r_{60}^{-3} \, \varepsilon_0 \, K_e \quad . \tag{3.9}$$

It should be noted that for both spherical and cylindrical geometries the field gradient is directed toward the central electrode resulting in DEP collection of particles at the electrode surface. However, in the case of the isomotive geometry, the gradient does not direct DEP motion toward electrode surfaces. This prevents sample build up on the electrodes. Practically speaking, this is particularly convenient for a continuous DEP system as the field conditions may be varied without washing the electrodes or flushing the system out between readings.

The isomotive electrode geometry is far less easily attained than the others. It is for this reason that most studies until now have used the simpler geometries.

In order to apply DEP one must take into account the mechanical properties of the system as well as the dielectric properties. For instance, with an iso-

Figure 3.4:

Isomotive electrode geometry in cross-section.

motive chamber filled with fluid and containing a particle, the particle will be acted on by the DEP force but the drag of the fluid on the particle surface will oppose the dielectrophoretic motion. For a fluid medium with viscosity η and an isomotive electrode geometry, a terminal velocity may be calculated at $\vec{F}_d = -\vec{F}_v$ where $\vec{F}_v$ is the fluid drag force[14, 1, 25]

$$|\vec{v}| = \frac{3a^2}{4\eta}V^2\, r_{60}^{-3}\, \varepsilon_0\, K_e \qquad (3.10)$$

where V is the electrode terminal voltage and r_{60} is a scaling factor for the electrodes. This applies to particles restricted to the region where

$$r > 2a > 0 \quad and \quad \theta \approx 0$$

where a is the radius of the particle [25].

The permittivity of a material results from a number of mechanisms, both microscopic and macroscopic. This represents the polarisation of the materials under the influence of an applied field. Each polarisation mechanism operates in a different frequency region above which it does not contribute to the permittivity. Thus, in general, as frequency increases, the permittivity of a material (or non-homogeneous system) decreases in steps corresponding to the critical frequencies associated with each mechanism. Figure 2.1 illustrates this effect for the real permittivity spectrum of muscle tissue.

3.2. Polarisation

3.2.1. Microscopic View

An atom may be considered to consist of a positively charged nucleus and surrounding negatively charged electrons in their appropriate orbitals centred about the nucleus (Figure 3.5a). When an electric field is applied the electrons tend to be pulled in the direction opposing the field, distorting the orbitals (Figure 3.5b). Thus the centre, or mean location, of the electrons is not identical with the nucleus resulting in a net electric dipole moment. This is known as *electronic polarisation* [1,28]. Each atom thus contributes an *electric dipole moment* equal to the magnitude of the charge of one sign times the distance between the charge centres.

When multiple atoms form into molecules the electronic charge will spend more time near some nuclei than others, thus, depending on the symmetry of the molecule, there may be no fixed dipole moment (highly symmetrical molecules eg. $C\,Cl_4$ Figure 3.6a) or a strong fixed dipole moment (asymmetrical molecules eg. $H_2\,O$ - $\vec{\mu} \approx 2\,D$ for liquid phase at 20 C [24], - Figure 3.6b; numerous proteins - $\vec{\mu} \approx 68000\,D$ for haemoglobin; and other biological molecules). This is known as the *permanent dipole moment* of the molecule, and is independent of externally applied field. Large molecules may have portions which are polar and other portions which are non-polar (such as the lipids).

When an external field is applied a torque is exerted on the dipoles tending to align them with the field. The freedom to align is regulated by

(a)

(b)
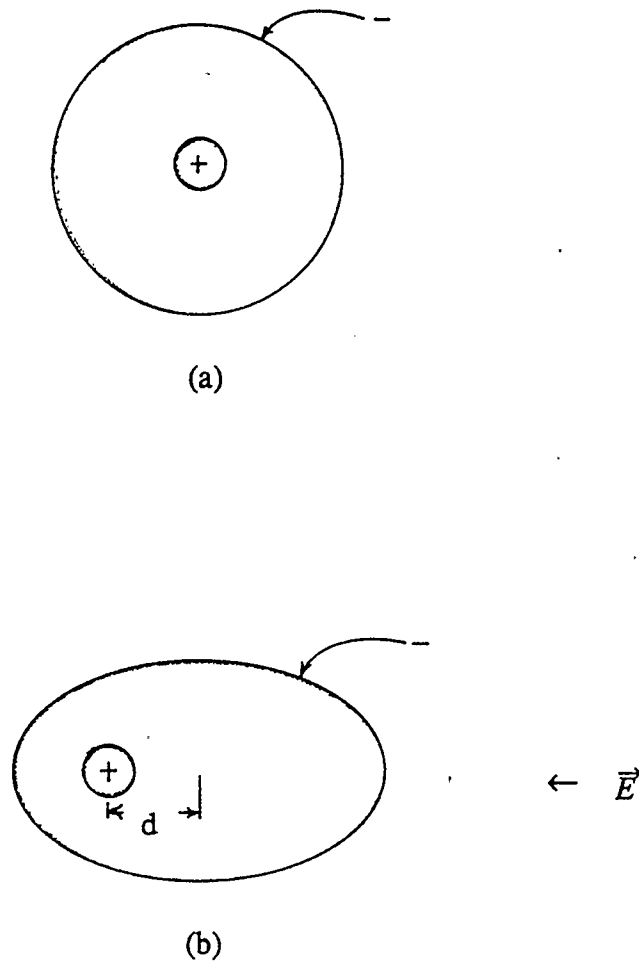
Figure 3.5:

Electronic polarisation model [28]

(a)   simple atomic model with no applied field

(b)   applied field causes distortion of electron orbitals resulting in polarisation.
      The net dipole moment is $\vec{\mu}$, where $| \vec{\mu} | = dq$.
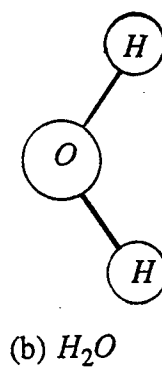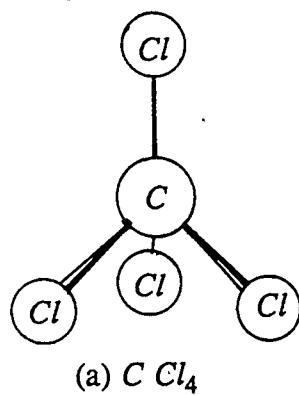
Figure 3.6:

Molecular polarisation

(a) $C Cl_4$ - no net dipole moment due to symmetry

(b) H_2O - asymmetrcal molecule has strong dipole moment.

interference with adjacent molecules and is high in gas, moderate in liquids, and very minimal in solids (see Figure 3.7). Polarisation of this type is termed *Debye* or *orientation polarisation* [28].

The bond lengths and angles within the molecules will fluctuate under the influence of an applied electric field. The resulting stretching, flexing, and rotation requires energy and may appear as a resonance dispersion. This is referred to as *atomic polarisation*.

Each of these microscopic mechanisms result in a frequency dependent polarisation, i.e. there is some frequency of applied electric field ($\omega_{cr} = 2 \pi f_{cr}$) beyond which the polarisation mechanism cannot keep up to the changing field. For electronic polarisation this occurs in the optical range and therefore does not concern us. Similarly the atomic polarisation dispersion is observed in the infrared frequencies and therefore is beyond the range of our instrumentation. Others, however, appear as a frequency dependent complex permittivity of the form

$$\varepsilon^* = \varepsilon'_\infty + \frac{\varepsilon'_s - \varepsilon'_\infty}{1 + j\omega\tau} \qquad (3.11)$$

where ε'_∞ is the real portion of ε at high frequency and ε'_s is the real part of ε at low frequency, $j = \sqrt{-1}$, ω is the angular frequency of the applied field and τ is the characteristic *relaxation* time of the polarisation mechanism. This is known as the Debye type relaxation for an ideal dielectric[1] and applies to a single relaxation process. For the case of Debye polarisation in water
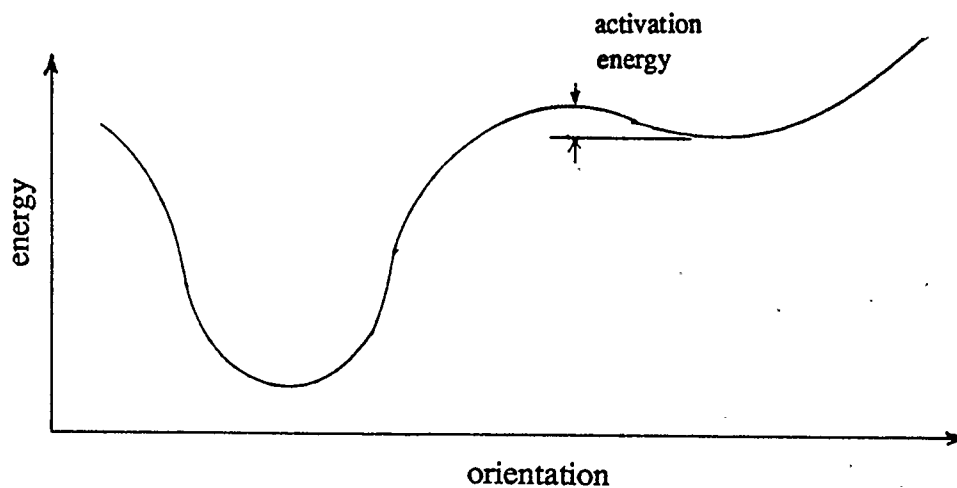
Figure 3.7:

Energy *versus* orientation for a polar molecule in an external field including interaction with local molecules. (The energy minimum need not occur when the dipole is exactly parallel to the applied field.)

The following applies to Figure 3.8.

$f_{cr} = 20GHz$ whereas for hemoglobin $f_{cr} = 1MHz$.

Experimentally the frequency at which a permittivity undergoes rapid change is called the *dispersion* frequency. For a single relaxation mechanism this is identical to ω_{cr}; however, multiple relaxation processes in the same frequency region, appear as a single broad dispersion. Figure 3.8a illustrates the permittivity spectrum for a single relaxation mechanism. Figure 3.8b shows the effect of three relaxations acting in the same frequency region.

In addition to the polarisation mechanisms which act only at the molecular level, there are numerous effects which take place at the interface between dissimilar materials. These effects, associated with macroscopic structures, are important in dealing with particles in suspension and particularly so when the particles are complex, as is the case for biological cells.

3.2.2. Macroscopic View

If a parallel plate capacitor is constructed with a large electrode area (A) compared to the electrode spacing (d) and is initially evacuated, the current through the capacitor will be described by

$$i(t) = C_0 \frac{dv(t)}{dt} \tag{3.12}$$

where C_0 is the free-space capacitance and may be described by

$$C_0 \approx \frac{A}{d} \varepsilon_0 \tag{3.13}$$

where ε_0 is defined as the permittivity of free space. If the evacuated gap is
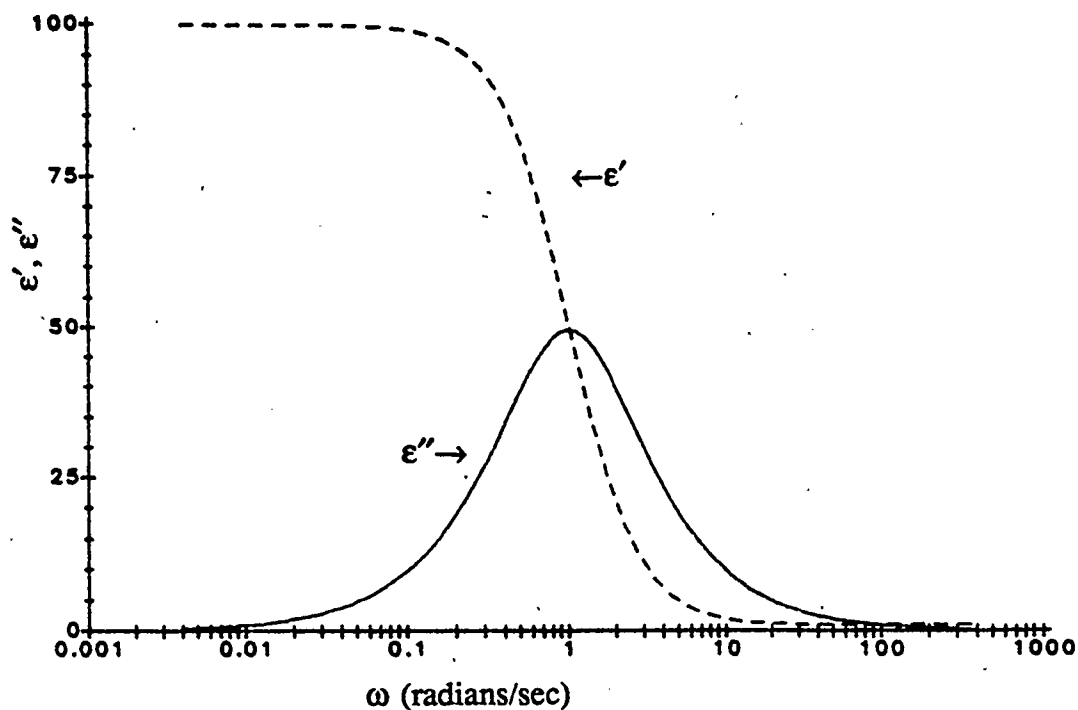
(a) single relaxation ($\tau = 1$ sec)

0.8)
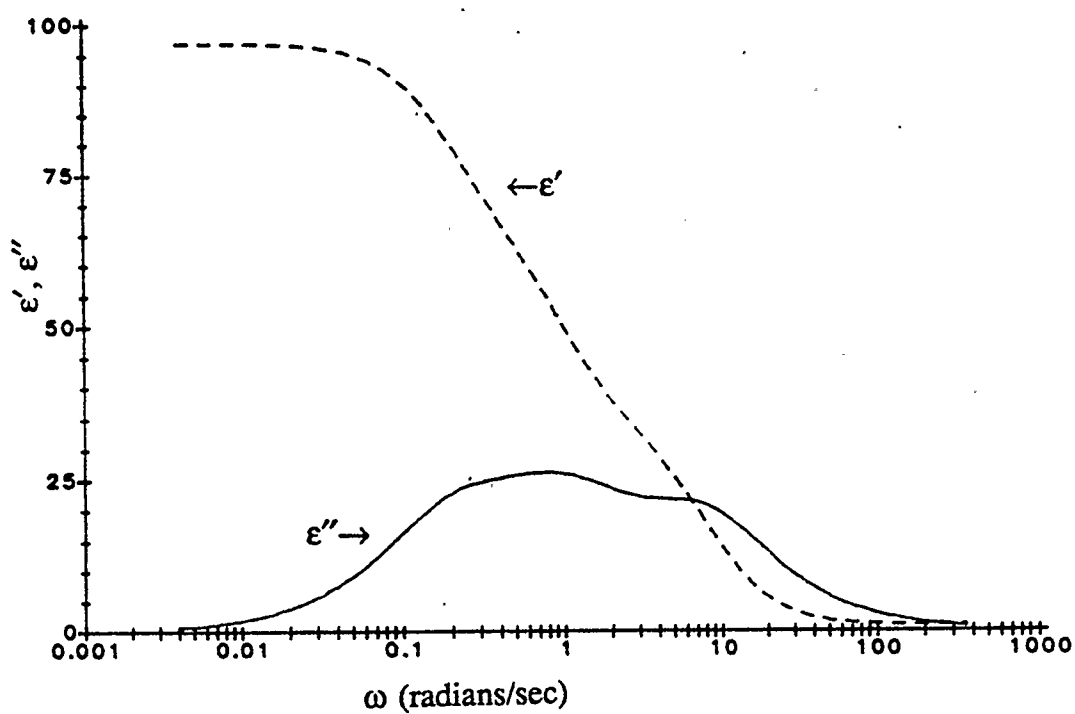
(b) triple relaxation ($\tau = 0.2, 1, 0.8$ sec)

Figure 3.8:

a)   single relaxation : single dispersion

b)   multiple relaxations : single dispersion

now filled by an ideal (lossless) dielectric and a new capacitance, C_1, is measured. The relative permittivity, ε_r, of the material may be determined

$$\varepsilon_r \approx \frac{C_1}{C_0} \qquad (3.14)$$

For a homogeneous medium , the permittivity may be related to the microscopic polarisabilities discussed earlier by

$$\vec{D} = \vec{E}\,\varepsilon_r\,\varepsilon_0 \qquad (3.15)$$

where $\vec{D}$ is known as the electric flux density[28] and

$$\vec{P} = \vec{D} - \varepsilon_0\,\vec{E} = \vec{E}\,\varepsilon_0\,(\varepsilon_r - 1) \qquad (3.16)$$

is the electric dipole moment per unit volume.

If this material is replaced by a conducting material, using the same experimental procedure we find the complex capacitance

$$C^* = C - j\frac{G}{\omega} \qquad (3.17)$$

where G is the conductance of the new capacitor, and the resulting permittivity is a complex quantity

$$\varepsilon^* = \varepsilon' - j\frac{\sigma}{\omega} \qquad (3.18)$$

where σ is the frequency dependent conductivity of the material. To more accurately model all of the possible loss mechanisms involved, the permittivity may be described as

$$\varepsilon^* = \varepsilon' - j\frac{\sigma_s}{\omega} - j\varepsilon'' \qquad (3.19)$$

where $\sigma_s = \lim_{\omega \to 0} \sigma$, and ε'' represents dielectric loss mechanisms characteristic

of the material [29].

Now, taking this same parallel plate capacitor and replacing the dielectric material with a two-layer sandwich of different materials, each having finite permittivities (ε_1 and ε_2) and conductivities (σ_1 and σ_2) and having thicknesses d_1 and d_2 such that

$$d = d_1 + d_2 \qquad (3.20)$$

(see Figure 3.9) we may model the system in this case as two leaky capacitors in series [1, 28]. These results may be interpreted[29, 30, 1] in terms of a single parallel plate capacitor of the original dimensions filled with a medium of frequency dependent permittivity and conductivity.

In this case the loss term, ε'', will reach a maximum at a critical frequency

$$\omega_{cr} = \frac{\sigma_1 d_2 + \sigma_2 d_1}{\varepsilon_1 d_2 + \varepsilon_2 d_1} \qquad (3.21)$$

where ε and σ represent the permittivity and conductivity of the respective materials and the subscripts 1 and 2 represent the two layers. This is known as Maxwell-Wagner polarisation.

This analysis has been extended[31] to obtain equivalent bulk parameters for the case of spherical particles in uniform suspension within a medium. It is found that the equation describing the permittivity spectrum is identical to the Debye relaxation spectrum with an additional conductivity term[13]

$$\varepsilon = \varepsilon'_\infty + \frac{\varepsilon'_s - \varepsilon'_\infty}{1 + j\omega\tau} - j\frac{\sigma}{\omega} \qquad (3.22)$$
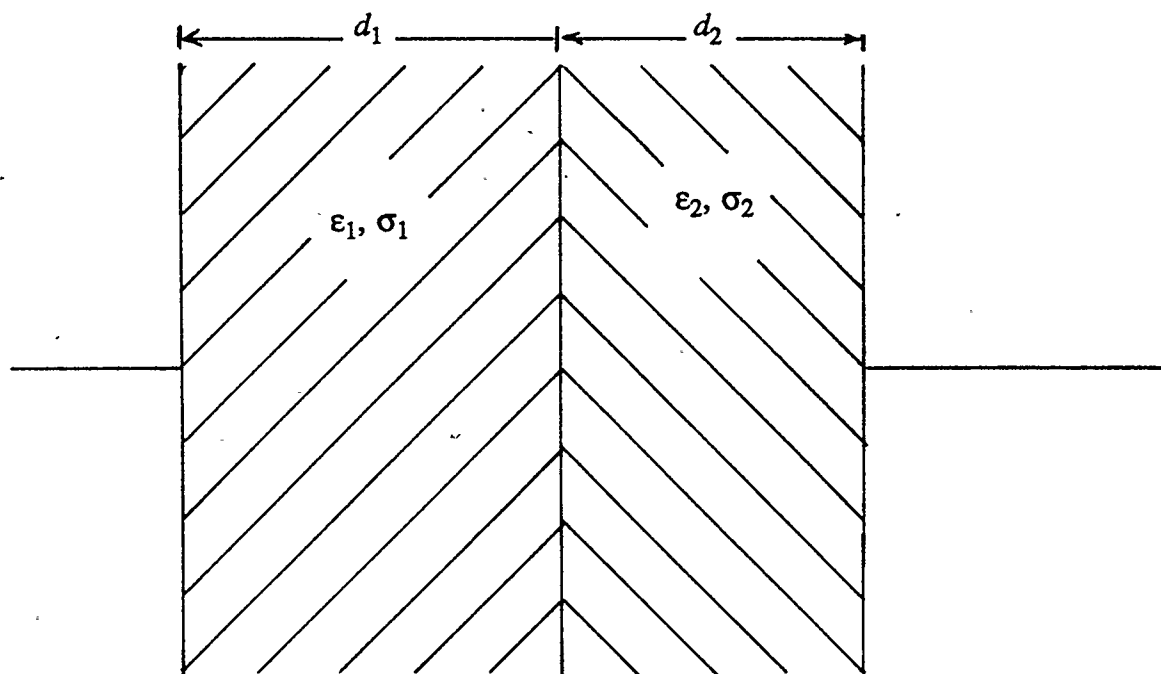
(a) 2-layer capacitor
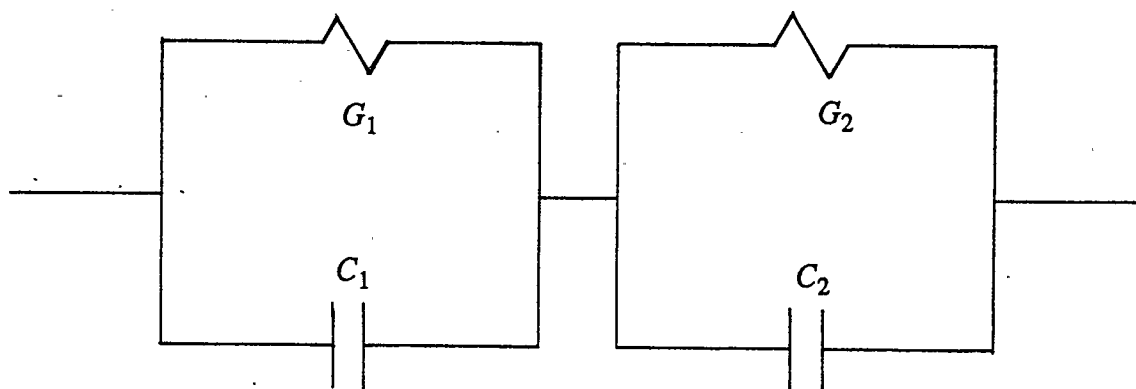
(b) equivalent electric circuit model

Figure 3.9:

Maxwell-Wagner (interfacial) polarisation.

where

$$\tau = \frac{2\varepsilon_1 + \varepsilon_2 - 2v_2\,(\varepsilon_1 - \varepsilon_2)}{2\sigma_1 + \sigma_2 + v_2\,(\sigma_1 - \sigma_2)}\,\varepsilon_0 \quad ;$$

$v_2 = $ *volume concentration of particles* ;

$\varepsilon'_\infty = $ *high frequency limit of the real permittivity*

$\varepsilon'_s = $ *low frequency limit of the real permittivity*

$\varepsilon_1,\ \varepsilon_2 = $ *permittivities of medium, particles*

$\sigma_1,\ \sigma_2 = $ *conductivities of medium, particles*

and

$$\sigma = \sigma_1\,\frac{2\sigma_1 + \sigma_2 - 2v_2\,(\sigma_1 - \sigma_2)}{2\sigma_1 + \sigma_2 + v_2\,(\sigma_1 - \sigma_2)} \quad . \tag{3.23}$$

The time constant ($\tau = 1/\omega_{cr} = 1/\,(2\pi\,f_{cr})$) represents the time taken for charge to accumulate at the interface. The thickness of this surface charge layer is considered[13] to be of the order of the Debye screening length, the distance from the centre of the concentrated charge region to a point at which the potential is e^{-1} of the value at the centre[13]

$$\lambda_D = \left[\frac{\varepsilon_r\varepsilon_0 kT}{2nq_e^2}\right]^{1/2} \tag{3.24}$$

where

$k = $ *Boltzman's constant;*

$T = $ *absolute temperature;*

$n = $ *free charge carrier concentration;*

and

$q_e = electronic\ charge.$

Further extensions have been performed for spherical particles with one shell, ellipsoidal particles, ellipsoidal particles with one shell and spherical particles with multiple shells [32]. It has been found that for any number of layers, or shells (n), in general $(n - 1)$ relaxation times will be observed. When dealing with ellipsoidal particles the permittivity becomes dependent on the particle orientation and geometrical factors (axial ratios). This is taken into account by inclusion of a *depolarisation factor* [13,32,33].

Should a particle have a net charge, a counterion cloud will form about the particle. The distortion of the counterion layer under the influence of an applied field results in yet another polarisation mechanism. Dukhin[29] has analysed the effect of counterions in terms of both a tightly bound and a diffuse layer of charge.

The bound-layer polarisation, first proposed by Schwarz [34], contributes an additional low-frequency permittivity of

$$\Delta\varepsilon_{bl} = \frac{9}{4}\left[\frac{v\ q^2\ a\ \rho_0}{1 + (v/2)^2\ \varepsilon_0\ kT}\right] \qquad (3.25)$$

and exhibits the Debye type relaxation described earlier with an associated time constant of

$$\tau_{bl} = \frac{a^2}{2\ u_b\ kT} \qquad (3.26)$$

where u_b is the mechanical mobility of counterions of surface density ρ_0 of

negligible thickness, v is the particle concentration per unit volume, and a is the particle radius.

The charge sites on the particle surface are essentially fixed, therefore an energy barrier, β, will have to be overcome in order for a counterion charge to move between sites, thus the bound layer charge mobility may be described as

$$u_b = u_0 \, e^{\frac{-\beta}{kT}} \tag{3.27}$$

where u_0 is the solution-mobility of the ions. A distribution of β (activation energy) values has been hypothesised to explain the broadening of the dispersion from that typical of a single Debye type relaxation [34].

This approach is very similar to that of Lewis[35] in which he proposes a *charge hopping model* for permittivities of non-crystalline solids.

This does not take into account the existence of a diffuse counterion cloud. In order to account for this, the above values of τ_{bl} and $\Delta\varepsilon_{bl}$ were adjusted by a factor of $\frac{1}{M}$ [1] where M is a function of positive and negative ionic charges, surface charge density, ionic concentration, and Debye shielding length of the diffuse layer. The diffuse layer thus contributes another low frequency increment in permittivity[1, 29], $\Delta\varepsilon_{dl}$ with an associated time constant of the order of

$$\tau_{dl} \approx \frac{a^2}{2D} \cdot \frac{1}{M} \tag{3.28}$$

where D is the diffusion coefficient of the counterions (and is temperature

dependent).

This refinement provides a mechanism to explain a shift toward higher frequency dispersion and reduced low frequency dielectric permittivity relative to those predicted by the bound-layer theory.

In biological systems there are numerous other mechanisms which have been proposed, the effects of which are difficult to predict due to the inherent complexity of biological cell structures. Among these mechanisms are

Nomadic polarisation

- yet to be isolated in biological systems

- takes place when charge carriers are free to roam the length of polymeric chains or structures of polymers

- potential structures within cells include DNA, microtubules, microfilaments, and long chain polymers such as actin and myosin.

Membrane polarisation

- has been isolated in synthetic membrane systems, such as purified egg lecithin bimolecular lipid membranes (BLM)[13]

- dispersion for these systems has been found to be in the region of 2 to 20 *kHz*.

Plasmoidal polarisation

- May take place within the cell wall of plant cells and certain bacteria

- involves low velocity migration of ions within the matrix of the cell wall[1]

- may also take place in the glycocalyx (or *fuzzy coat*) of mammalian cells

- independent of surface charge density

- theory predicts[1] the relaxation time, τ, is given by

$$\tau = \frac{a^2}{2ukT} \qquad (3.29)$$

and the increment in effective permittivity

$$\Delta K_e = f(\tau, \varepsilon_2, N) \qquad (3.30)$$

where N is the ionic concentration, a is the particle radius, and u is the ionic mobility within the glycocalyx (fuzzy coat) of the cell.

Table 3.1 contains a summary of the pertinent aspects of each mechanism discussed here.

As has been pointed out by Daniel [36], although a thorough understanding of the mechanisms involved at a microscopic level may allow predictions of dielectric properties, knowledge of these properties does not isolate a single mechanism. In practice dielectric measurements may, however, be used in conjunction with other techniques to gain an understanding of the underlying mechanisms.

Polarization Mechanism	ω_{cr}	Form	Temperature Dependence	Conductivity Dependence	Other
Electronic	optical (visible to ultraviolet)	resonance	none	none	
Atomic	near infrared	resonance			
orientation (Debye)	microwave to far infrared	relaxation (in liquid)	thermally activated	none	$\tau \alpha$ (η, *molecular diameter*)
Maxwell-Wagner	10^4 to 10^8 Hz	relaxation	none	τ dependent on both σ_1 and σ_2	τ dependent on number of dielectric particles per unit volume
bound-layer counterion	10 to 10^3 Hz	relaxation	thermally activated	$\epsilon \alpha$ ionic concentration	$\tau \alpha \dfrac{l^2}{D}$; ϵ dependent on particle concentration.
diffuse-layer counterion	low frequency (10 to 10^2 Hz)	relaxation	see temperature dependence of the diffusion coefficients of counterions	extremely complicated	$\tau_D \alpha \dfrac{l^2}{D} \times \dfrac{1}{M}$

Table 3.1:

Characteristics of major polarization mechanisms (note that $l \approx$ particle diameter; $\omega_{cr} = 1/\tau$ is the critical frequency range; D = the diffusion coefficient; η = viscosity)

CHAPTER 4

INSTRUMENT

4.1. Design Specification

This project was entered into with the following design objectives:

1) to develop a system to characterise particles, specifically biological cells, in terms of their dielectrophoretic response spectra

2) to do so with minimum disruption of samples and with maximum speed

3) to minimise operator intervention required in the measurement procedure (automate)

4) to facilitate dual cell characterisation and cell separation using the same system.

A continuous flow system was adopted, as opposed to the batch approach, as this lends itself to rapid measurements and automation. The isomotive electrode geometry was chosen to minimise sensitivity of the measurements to initial sample stream position, to allow a linear relationship between V^2 and stream displacement, and to allow measurement of both positive and negative DEP.

The system was designed to be constructed as a series of discrete modules in order to allow testing and modification of each segment without requiring

disruption of other portions of the system.

The initial conceptual design is shown in Figure 4.1, while Figure 4.2 illustrates the system in its final operational state. The major components selected to fulfill the requirements of the design are shown in Table 4.1.

4.2. Electrode Chamber

The dimensions of the electrode chamber were based on the calculations of Pohl, Kaler, and Pollock[14] which suggest that a value for r_{60} (Figure 3.3 and Equation 3.7) of 1 *mm* would be sufficient to give measurable deflections of the cell stream for electrode potentials of 10 V_{pp}.

These electrodes (152.4 *mm* in length) were machined from square brass rod (6.35 *mm* on a side) by a numerically controlled milling machine (Yasnac-Matsuura) with a stated repeatability of 3×10^{-4} *inches* (7 μm). Confirmation of this would require an optical comparator system which is currently unavailable. The electrodes were subsequently electroplated with gold to minimise electrode polarisation effects. They were then mounted in a sealed plexiglass chamber designed to match and seal with other modules in the system (see Figure 4.3).

4.3. Fluid System

Figure 4.4 schematically illustrates the final fluid system design.
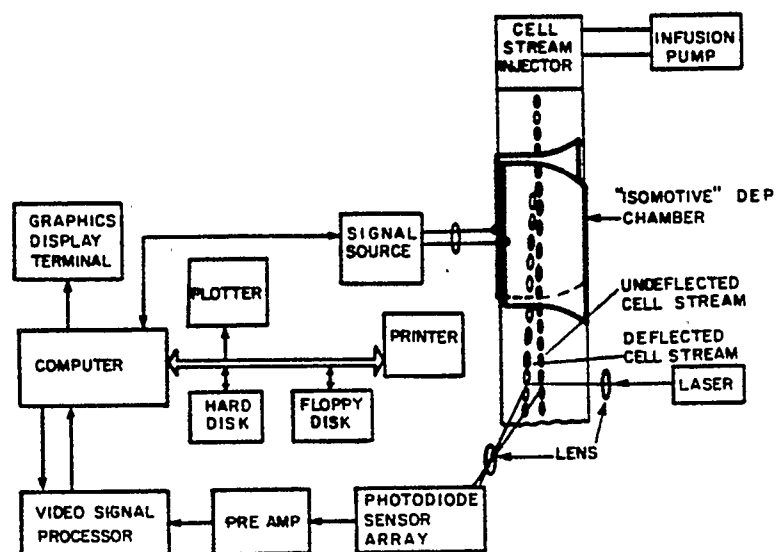
Figure 4.1:

Continuous DEP system - conceptual design

data acquisition processor   syringe pump   effluent flask   sheath syringe   sample syringe   bleeder syringe   injection chamber   electrode chamber

pre-amp

camera

signal source

computer system

laser

42
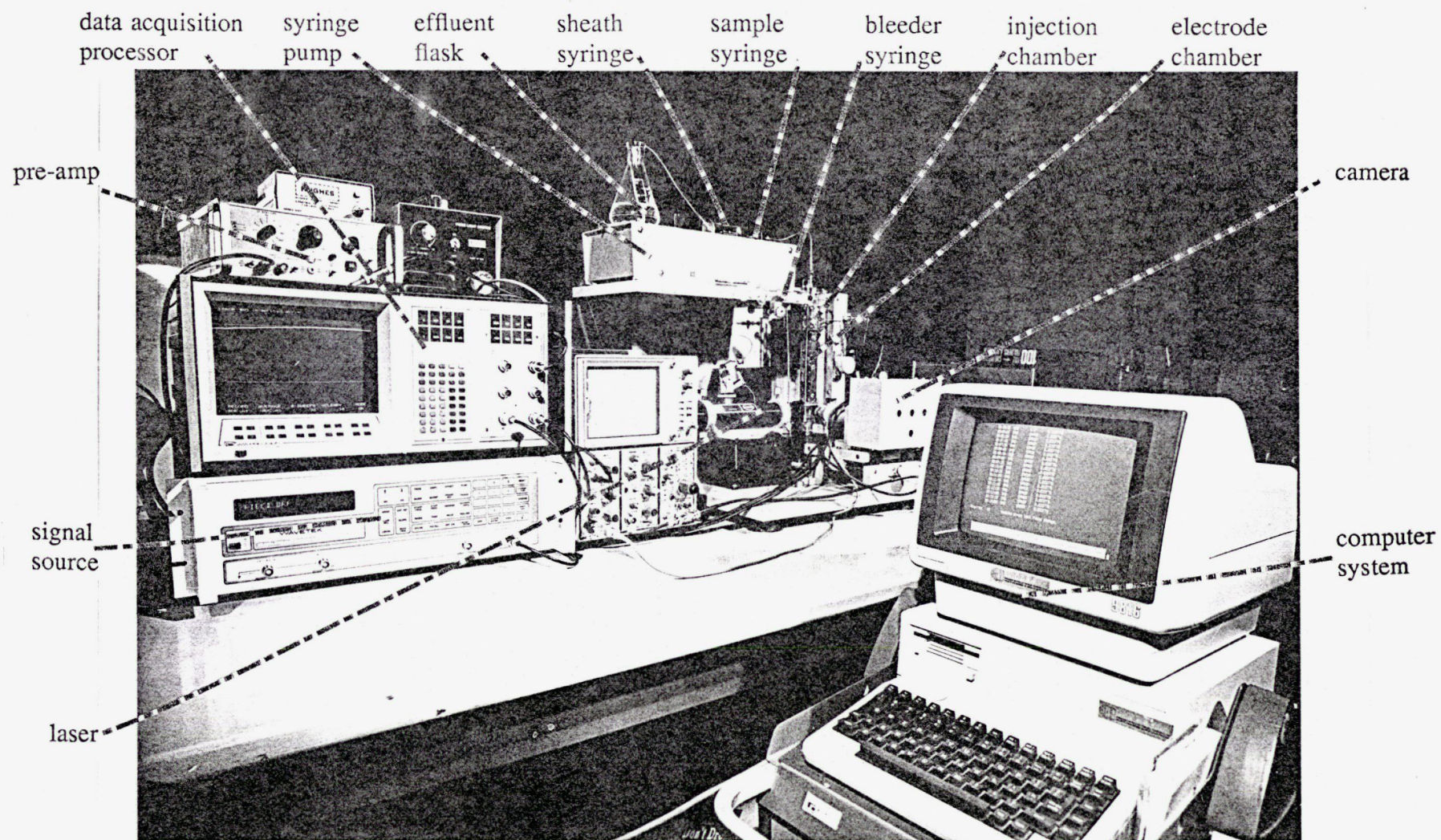
Figure 4.2:

Operational Design

Device	Description	Justification
electrode chamber	isomotive	- minimise position dependence of response (most linear geometry)
	wet electrodes	- maximise frequency range (useful below 1 kHz)
	$r_{60} = 1$ mm	- maximum deflections with available fields and machining techniques
	length = 6″ (152 mm)	- initial tradeoff between high enough flow rates to minimise settling effects and long enough period within the chamber
injector	"isomotive" shape #26 guage injection needle	- minimise fluid disruption on transition to electrode chamber - small diameter needle without producing excesive shear on the sample particles on passage through the orifice
	bleeder	- placed at tapered top of fluid chamber to allow removal of trapped air and to ease priming of the fluid system
fluid drive	infusion pump Harvard Apparatus HA975	- widely variable flow rate - ratio of sample to sheath flow rates fixed by ratio of syringe barrel diameters - smooth drive (little or no pulsing of the fluid)
optical detector	reticon 1024G (1024 mu 1 diode array)	- displacement is critical measurement thus 1D array sufficient - 1024 elements allows sufficient resolution over a wide enough area - sensitive detector
lens	Wild/Leitz 4/0.12	- large numerical apperture (0.12) thus minimum light loss - high enough optical magnification (mu4) to allow 6.25 μm position resolution
light source	HeNe laser 1.25 mW	- wavelength matches peak sensitivity of detector - high intensity - narrow beam
beam spreading lens	not required	- beam diameter of HeNe laser already appropriate - spreading beam would reduce flux density at scatterer
pre-amp	Princeton Applied Research	- variable gain ($mu10$ to $mu10000$) - variable bandwidth (3 to $3mu10^5$ Hz) - low noise
video signal / data acquisition processor	Data Precision Data 6000	- high acquisition rate (40 kHz) - synchronous sampling - ensemble averaging - programmable for internal signal processing - IEEE 488 bus control
signal source	Wavetek 178	- wide range of frequencies (0 to 50 MHz) - high output (up to 20 V_{pp}) - IEEE 488 bus control
computer; storeage; printer	HP9816	- 10 MB hard disk ; 450 kB minifloppy - dot matrix printer - IEEE 488 bus controller - graphics

Table 4.1 : Design choices and justification.
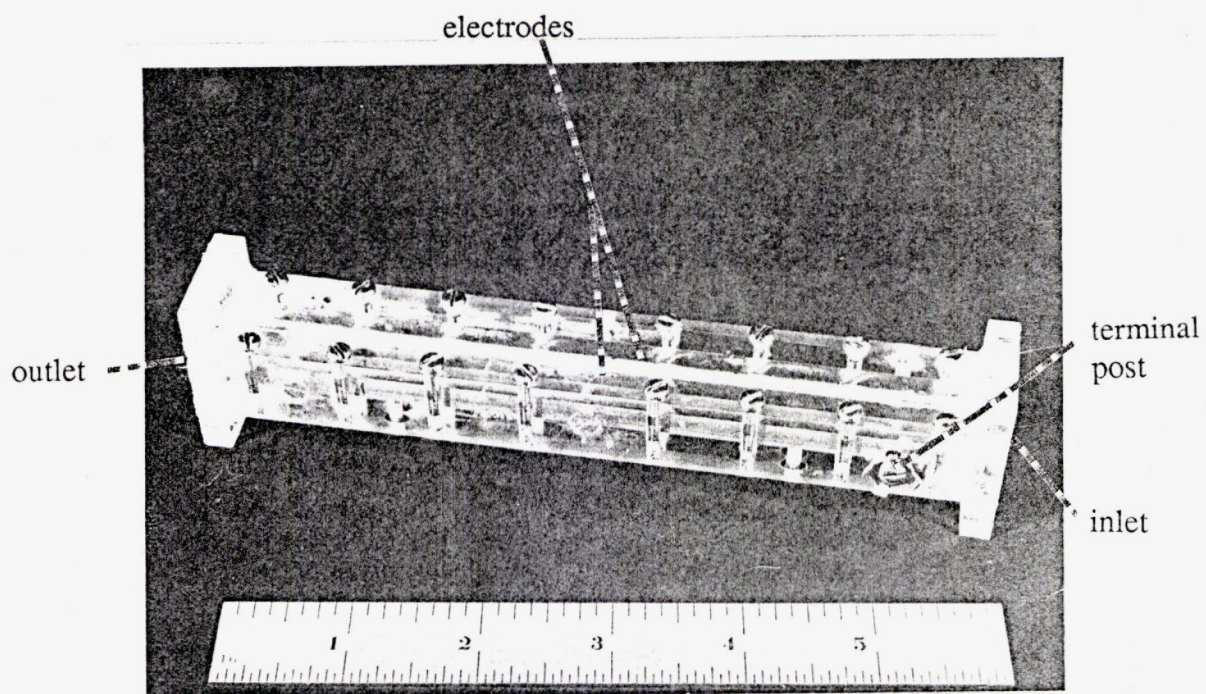
Figure 4.3:

Electrode chamber.

	INDEX
A	sample syringe
B	sheath syringe
C	bleeder syringe
D	bleeder stopcock
E	sheath stopcock
F	outlet stopcock
G	sheath port
H	bleeder port
I	injector needle
J	injection chamber
K	electrode chamber
L	observation chamber
M	outlet constriction
N	outlet port
O	effluent flask
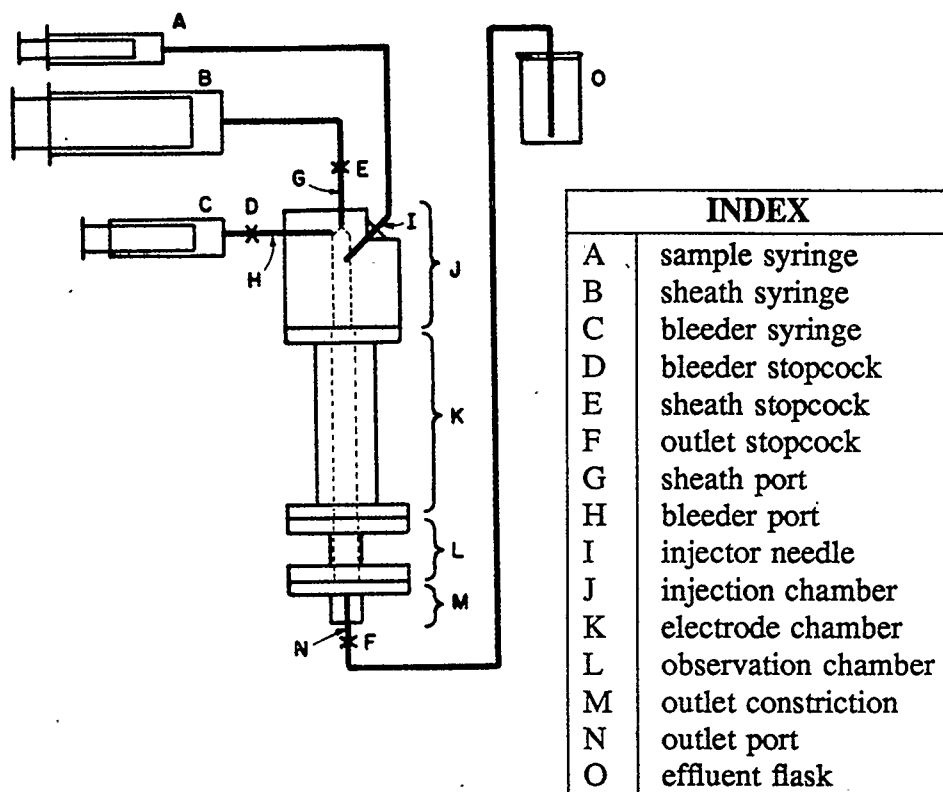
Figure 4.4:

Fluid system schematic.

The infusion pump drive system was chosen over gravity feed and pneumatic systems because the flow rate could be readily fixed by adjustment of the transmission setting. The infusion pump (Harvard Biosciences Compact Infusion Pump - HA 975) holds two syringes. The plungers are depressed at a constant rate by a single piston:

$$plunger\ velocity = 1.8269 \times 10^{-3} \cdot \left[712.85 \times 10^{-3}\right]^{n} \ m\ sec^{-1} \qquad (4.1)$$

where $0 < n \leq 30$ is the transmission setting. In this way the ratio of the sample to sheath flow rates is fixed by the ratio of syringe diameters.

Sample and sheath syringes (A and B in Figure 4.4) are mounted in the infusion pump. A third, bleeder, syringe (C) is provided to aid in flushing, priming, and removal of air bubbles which collect at the top of the injection chamber (J). The sheath flow enters at the top of the injection chamber via a #16 gauge needle (G). The sample is injected via a #26 gauge teflon needle (I) into the centre of the sheath flow, low enough down to ensure that the sheath flow is stable at the nominal operating flow rates. The injection point is adjustable along the centre line of the chamber. The cross section of the injection chamber follows the same contour as the electrode chamber (K) to minimise mixing at the transition between modules. The rectangular glass observation chamber (L), of the same approximate cross-section as the electrode chamber, is followed by the outlet constriction consisting of a #16 gauge needle (N). The effluent is deposited in a flask (O) at the same approximate height as the syringe pump. This provides positive pressure throughout the system and

prevents collection of air bubbles. Figure 4.5 illustrates the completed fluid system

A critical requirement of the fluid system, from injector to outlet, is that there be minimum mixing in order to maintain the sample stream as narrow as possible. This essentially means that laminar flow must be maintained [37].

Laminar flow occurs when the Reynolds number (Re), the ratio of viscous forces to inertial forces, is low (Re < 2000).

$$Re = \frac{UL}{\nu} \qquad (4.2)$$

where U = a characteristic velocity, L = characteristic distance, and ν = the kinematic viscosity of the fluid [38].

Assuming a circular cross-section of equivalent area (a conservative simplifying assumption) and using the resulting tube diameter (3 mm) for L, taking the typical velocity as the mean velocity at pump speed 10 (5 mm sec^{-1}) (most runs to date use pump speed 14, making the estimates here high by a factor of four ; see equation 4.1), and obtaining the kinematic viscosity for water at 25 C from tables[38] (10^{-6} m^2 sec^{-1}), we find a Reynolds number of approximately 15 (≪ 2000). It can therefore be stated with confidence that laminar flow is maintained throughout the system.

The simplifying assumption implicit in the preliminary design is that the flow velocity is independent of position within the isomotive chamber. This is obviously not the case. However the actual flow profile requires a numerical

sample syringe sheath syringe bleeder port and stopcock sheath stopcock and inlet sample injector infusion pump bleeder syringe tube to effluent flask
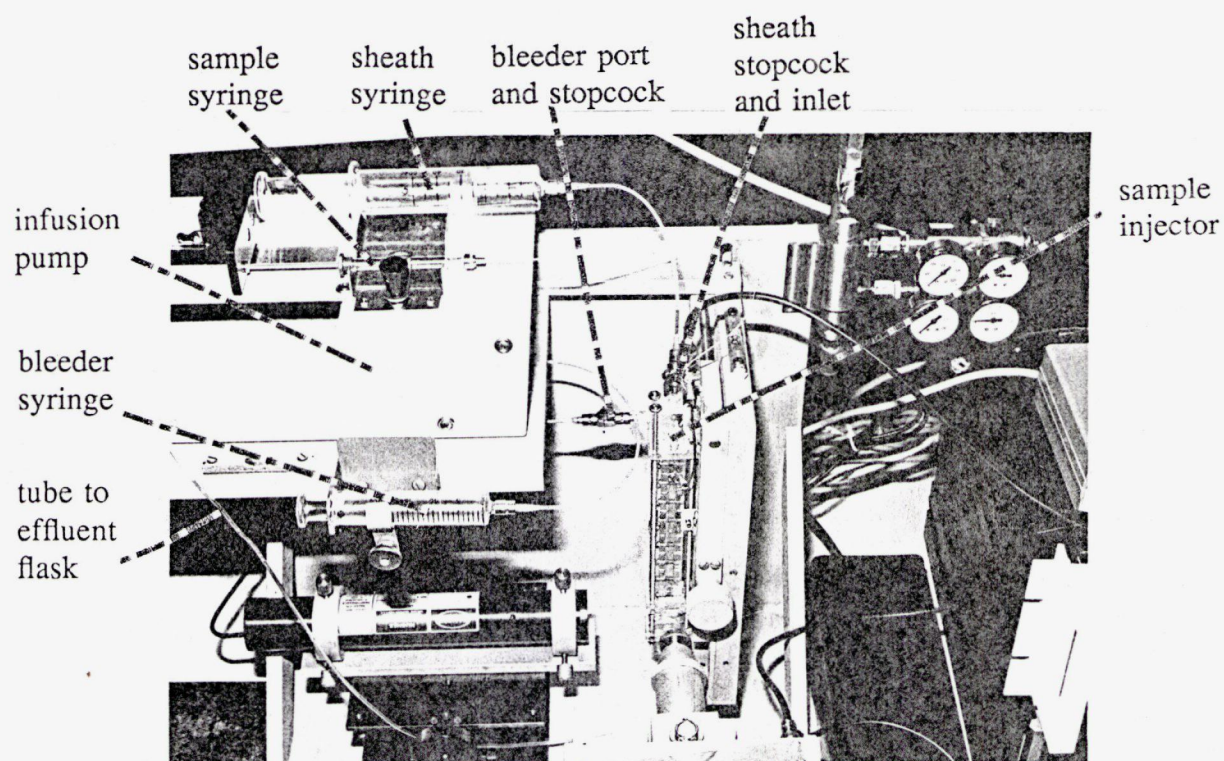
Figure 4.5:

Fluid System as implemented.

solution of Poisson's equation in two dimensions and has not been undertaken here. Qualitatively, however, it is expected that the velocity will be zero at the walls and higher in the broad regions than in the narrow ones due to viscous drag at the walls. An approximate sketch of the expected flow profile is shown in Figure 4.6.

As mentioned above the injection chamber is of the same cross-section as that of the electrode chamber. A teflon needle injects the sample stream at a variable position along the centre line of the chamber. When the end of the needle is trimmed perpendicular to its length a slight pressure drop appears just below the top edge of the needle outlet (see Figure 4.7). This pulls a portion of the sample flow out from the bottom edge of the needle orifice broadening the stream. Trimming the top edge away removes this low pressure region and results in a much narrower and more stable stream; however, needle orientation becomes critical.

4.4. Optical System

As the diameter of the particles to be studied ranges from 4 μm to 50 μm, it was estimated that the limit of useful resolution for position detection would be approximately 5 μm.

The usable area of the isomotive chamber was estimated to be of the order of 2 to 4 mm thus a 1024 element diode array with a resolution of 5 μm (covering an effective range within the observation chamber of 5.12 mm) could be

(a)

(b)
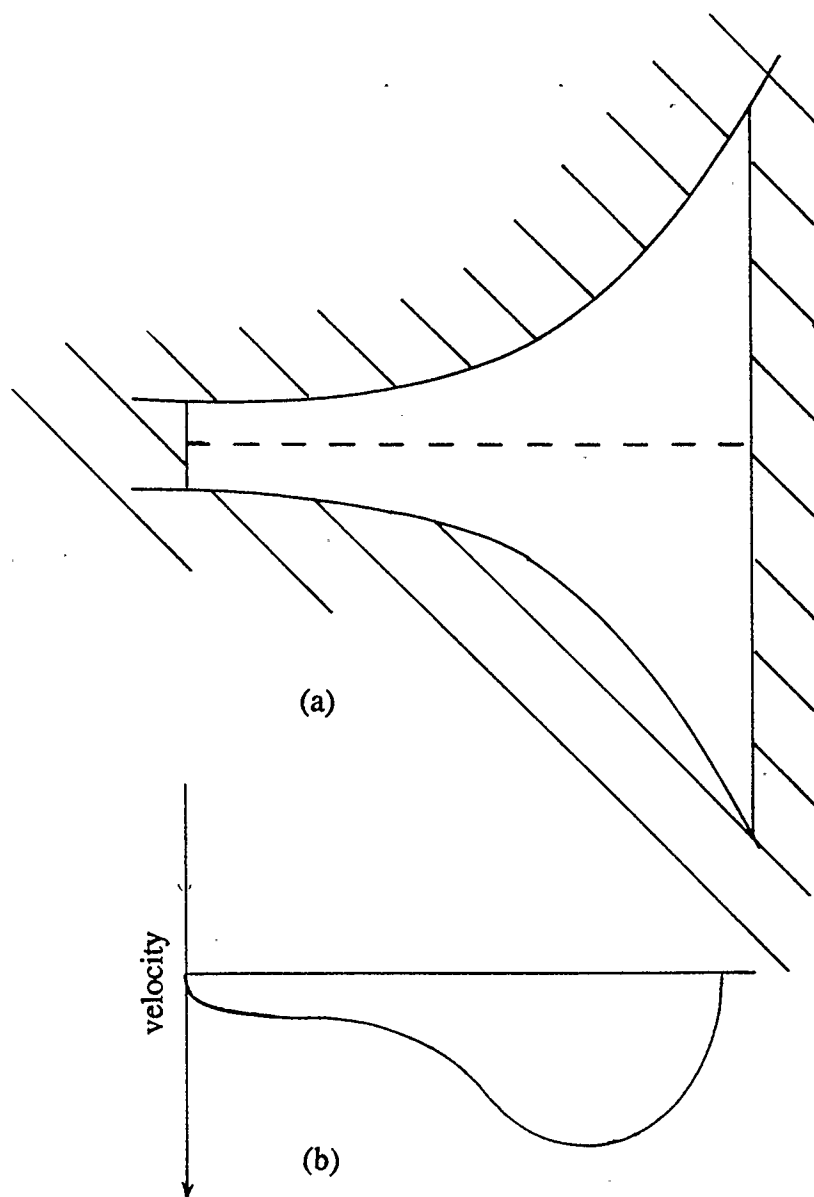
Figure 4.6:

(a)   electrode chamber cross section

(b)   estimated flow profile along centre line of electrode chamber.

pressure drop

pressure drop

(a)

pressure drop

(b)
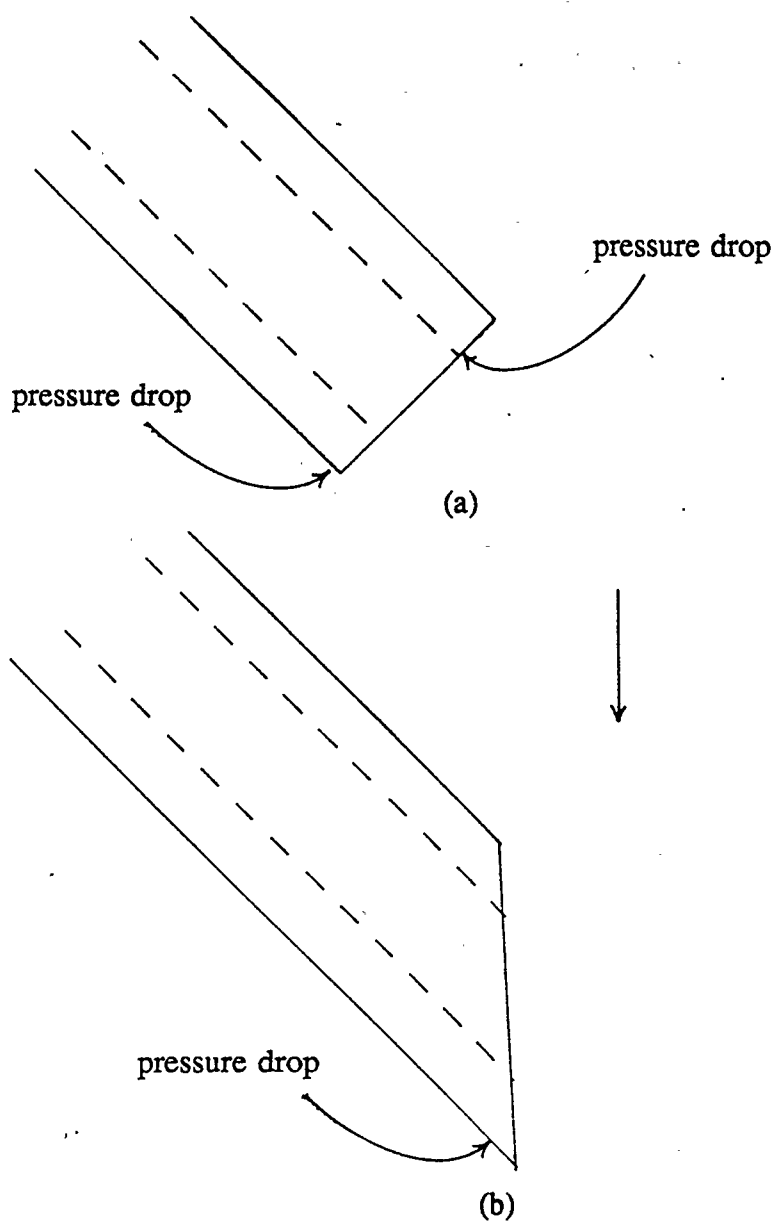
Figure 4.7:

Injector design

(a) double low pressure regions broaden the stream

(b) trimming the needle tip eliminates one low pressure region thus narrowing the
stream.

adjusted to the centre of the usable region and left. The 1024 element Reticon 1024G diode array provides a detector of fairly high peak sensitivity $(0.4192 \ A \ W^{-1})$ and 25 μm square pixels.

To obtain 5 μm resolution an optical magnification 5 x would be required. Additional constraints, however, were that the minimum amount of light was to be lost and a working distance of 25 mm was required. The best tradeoff of these parameters was to be obtained with the Wild/Leitz 4/0.12 microscope lens with a numerical aperture of 0.12 and a magnification factor of 4x (working distance $\approx$ 25 mm). This fixed the optical resolution at 6.25 μm. Figure 4.8 illustrates schematically the final detector system design and Figure 4.9 illustrates the physical layout of the components.

The cell stream is illuminated via the wall perpendicular to the detection window. In this way a high contrast signal of bright spots on a dark background could be detected taking full advantage of the available spatial resolution.

A 1.25 mW HeNe laser (Hughes) serves as the required high intensity light source. The wavelength of the laser (635 nm) is within the peak detection efficiency of the Reticon array (*peak* $\approx$ 750 nm), yet is still within the visible range simplifying alignment and focusing. At this wavelength the array achieves a quantum efficiency of 79.98 % and the sensitivity is 0.4192 $A \ W^{-1}$ (93 % of that at the 750 nm peak efficiency). The camera electronics, detector, and optics system are mounted on an x-y carriage assembly (see Figures 4.9
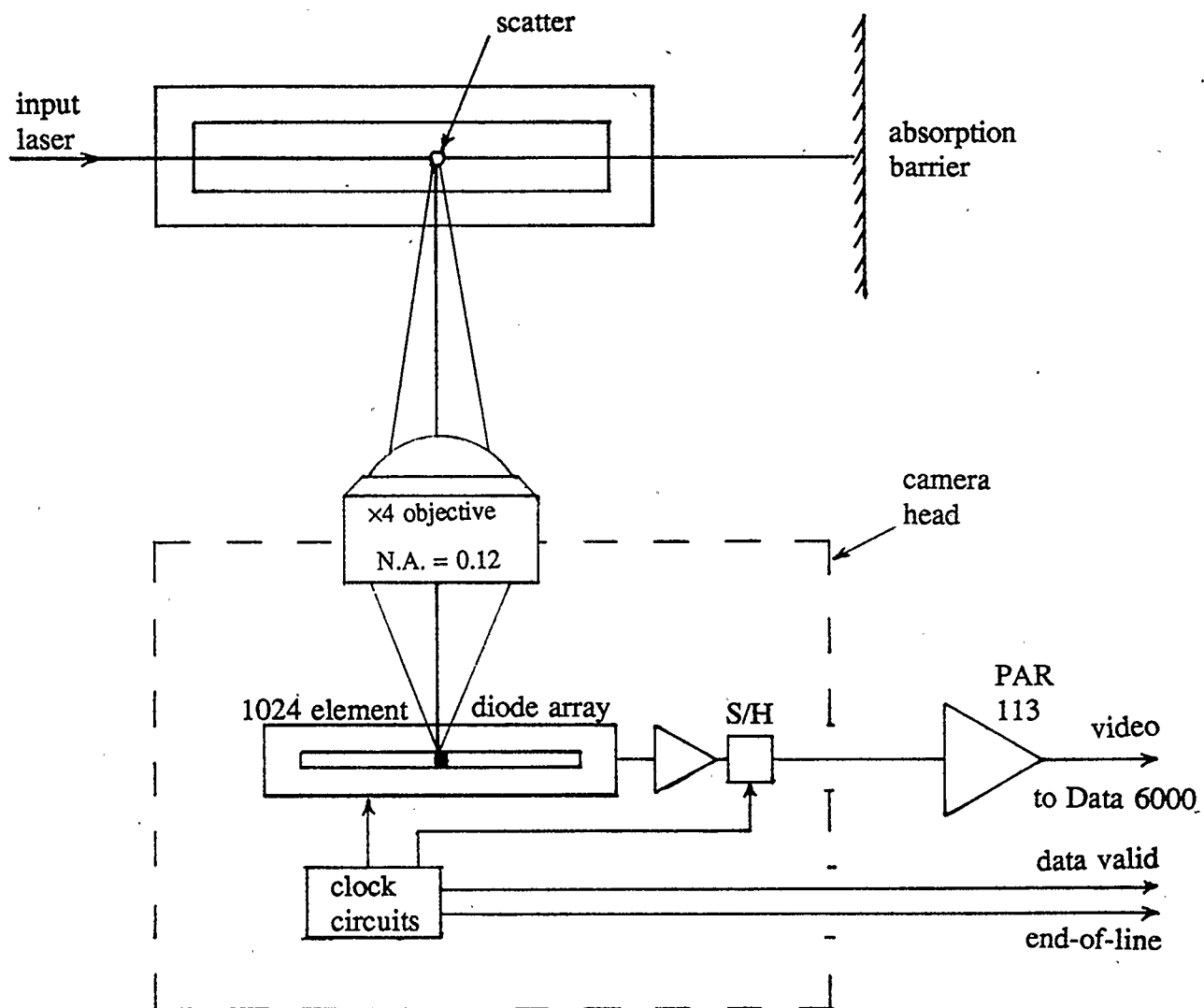
Figure 4.8:

Detection system schematic.

54
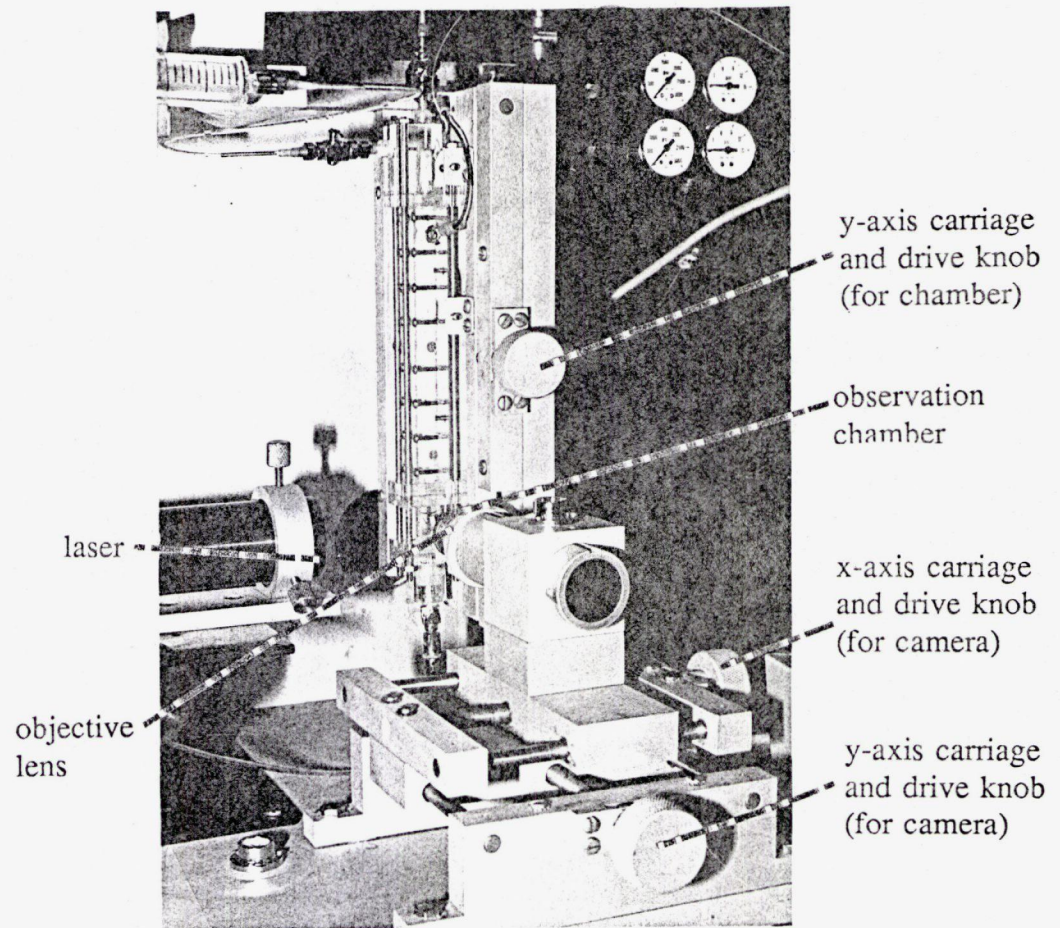
Figure 4.9:

Optics System (camera box removed).

and 4.10), which was designed and constructed in house, to allow focusing and alignment with the sample stream.

The observation chamber, Figure 4.11, is rectangular due to the difficulty of achieving an isomotive cross-section in glass. The cross-sectional area of the observation and the electrode chambers are approximately the same. The laser beam passes through the narrow side of the chamber and light, scattered by the particles in the sample stream, is detected through the broad window.

In order to provide alignment of the laser with the edge of the observation chamber the entire chamber system is mounted on a y-axis carriage on the vertical cantilever (clearly visible in Figures 4.9 and 4.10). The laser is mounted on a scissors jack to allow placement at precisely the same level as the detector (Figure 4.10).

4.5. Signal Processing

Due to the low intensity of the scattered light arriving at the detector integration of the optical signal in the imaging array is performed by reducing the clock rate to 8 *kHz* (the minimum rate at which it will operate consistently while successfully clearing out the accumulated dark current from the previous scan). This means that the charge integrates in the detector pixels for 1/8 second before readout effectively providing signal averaging for this period without addition of electronic noise from the signal chain. This video signal is then passed through a variable gain preamplifier, (Princeton Applied Research :

y-axis carriage
assembly

y-axis adjustment
knob

observation
chamber

objective
lens

laser height
adjustment

camera
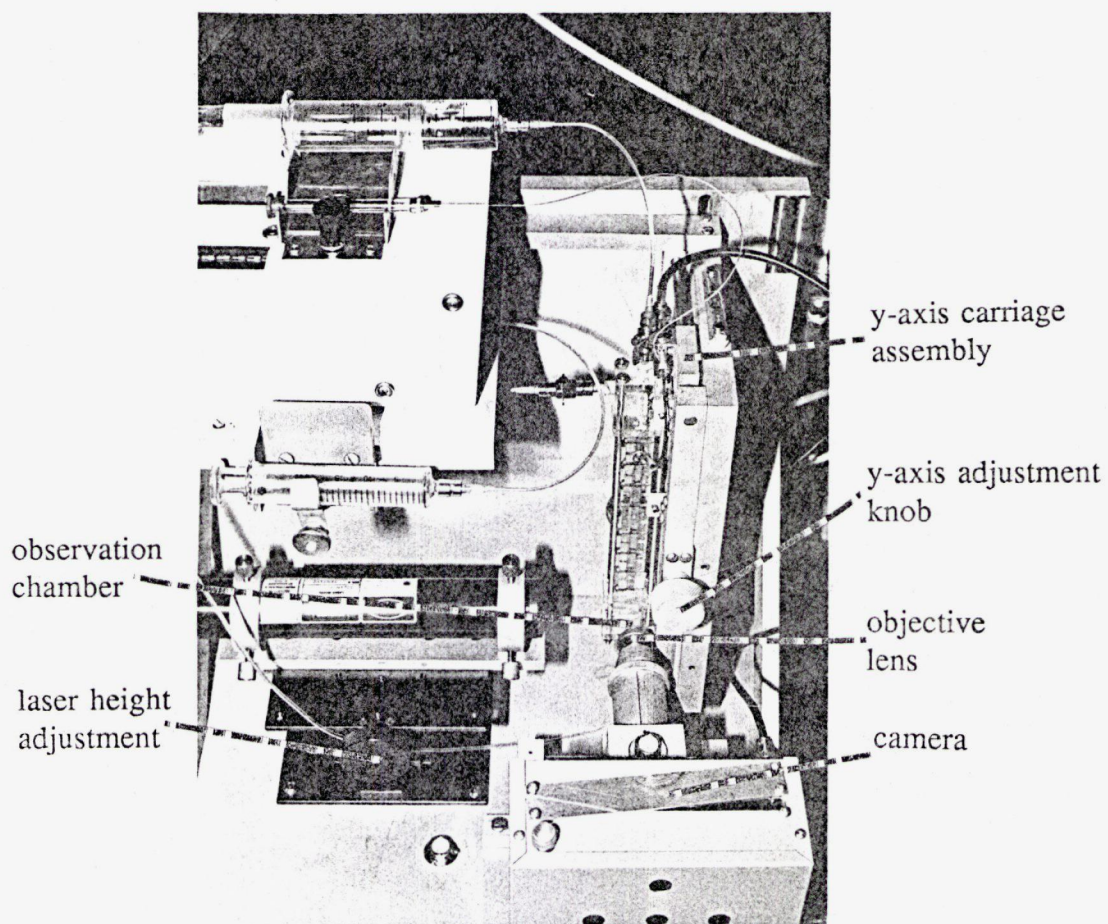
Figure 4.10:

Optics system - plan view.

57
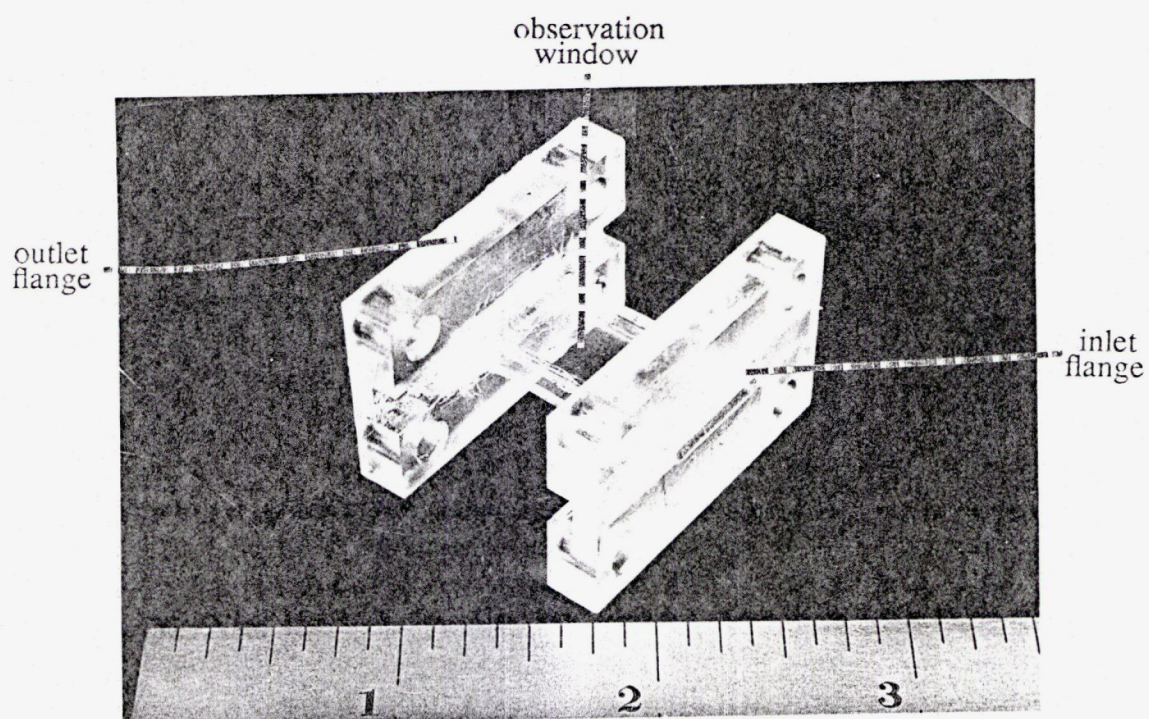
Figure 4.11:

Observation chamber.

PAR 113, set to ×10 or ×20) then sampled synchronously by the data acquisition/processor (Data Precision: Data 6000).

Due to processing limitations of the Data 6000 only every second scan is acquired. These are then averaged for 256 lines. This provides a clear indication of the stream position, however a precise peak location is difficult to determine due to noise superimposed on the signal.

At this point the Data 6000 performs a convolution with a ten point triangle wave. This smooths the data. However, some broadening of the peak results.

The stream location is then approximated to the peak location and the stream width is estimated to be the width half-way between the minimum and maximum value in the region of interest.

The parameters passed to the computer include location, width, and peak-to-peak signal strength.

Because of the long integration and averaging time this approach results in extremely conservative estimates of stream width as minor stream fluctuation during the averaging time shows up as a broader stream.

4.6. Automation

An HP 9816 desktop computer with an internal hard disk (10 MB), a minifloppy disk, and a dot matrix printer provide control of both the Wavetek 178 signal synthesizer and the Data 6000 data acquisition/processing system. A

simple software package has been written (in HP BASIC 3.0) to allow initialisation of the instruments, selection of desired signal frequency and amplitude for the signal source, and periodic acquisition and logging of selected parameters on the printer. These are usually time, stream location, stream width, and signal strength (pk-pk) and are acquired every 65 seconds (every time the Data 6000 completes 256 averages of the incoming data) or every 35 seconds for 128 averages.

For a more comprehensive description of the software and its operation the reader is referred to Appendices A and B.

4.7. Mechanical System

The frame on which the system is mounted has to be mechanically robust: it should be as rigid as possible to minimise the effects of vibration and to prevent accidental misalignment after setup, and it should be as flexible as possible to allow work or adjustment on any one portion of the system without major disruption to other sections.

These objectives were met by constructing the load-bearing frame of 3/4 " aluminum plate, heavily braced. The cantilever and pump shelf are both bolted to the back plate using knurled knobs for simple removal and adjustment. The mounting holes for these components are slotted to allow coarse adjustment of the height of both components.

The carriage on the cantilever, on which the entire chamber module is mounted, is a separate unit from the cantilever to allow separate adjustment and modification.

The x and y carriages under the camera system are almost identical modules mounted one atop the other at 90°. All carriages and the scissors jack under the laser are driven with knurled knobs.

The carriages and laser jack are firmly bolted to the base plate which is supported by four broad rubber feet selected to damp vibration from other sources in the environment. The pump is bolted to its adjustable shelf.

4.8. Calibration

Although empirical calibration of the system has not been done, it has been determined that the particles spend approximately 65sec between the electrodes at pump setting 14. Assuming that the stream displacement (x) is described by $v_x \times t$, and v_x is the transverse displacement velocity and is approximately constant, and using Equation 3.9, a constant may be obtained which relates the displacement to the effective permittivity:

$$K_e = 1.45 \times x \qquad (4.3)$$

where x is measured in pixels. This is obtained for 5 μm diameter spheres at 10 V_{pp} applied voltage in water ($\eta = 10^{-3}\ kg\ sec^{-1}\ m^{-1}$), and with electrodes of $r_{60} = 1\ mm$.

CHAPTER 5

TESTING

The preliminary testing of the instrument covers several areas such as average stream boundaries, stream stability, minimum and maximum flow settings, and their effects on stream boundaries, and acceptable sample suspension concentrations.

In addition to these, testing of the functionality of the system has taken place in which the displacement *vs* V^2 dependence was determined (see Equation 3.8), spectra were obtained for yeast (*Sacharomyces cerevesiae*) over a wide range of frequencies, with different medium conductivities. DEP spectra were also obtained for polystyrene-DVB microspheres (Duke Scientific) 5 μm in diameter. (For procedures see Appendices A through C and E).

5.1. Stream Diameter

Because the stream is formed in the injection module (with "isomotive" cross section) and is monitored in the rectangular observation chamber, the original stream undergoes some distortion (see Figure 5.1). This distortion is dependent on the initial position of the stream. A circular stream injected where the chamber is *narrower* than the observation chamber will result in a *reduced* stream diameter at the observation chamber, if injected where the injection chamber is *wider* than the observation chamber the transition from
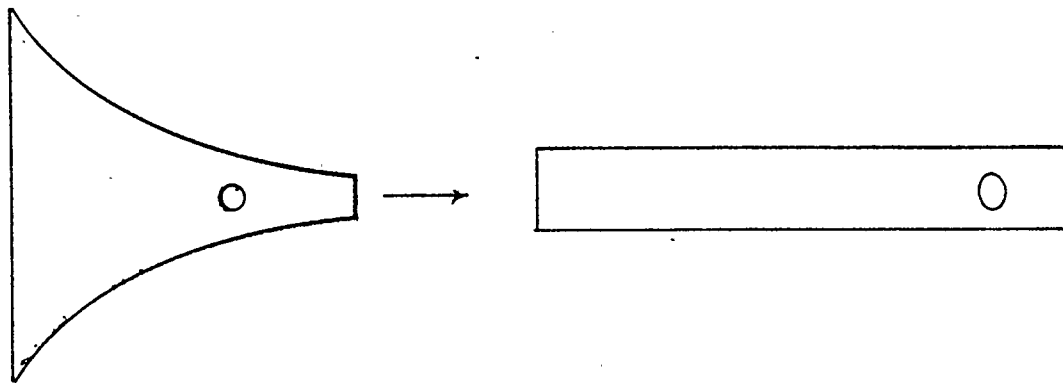
(a)
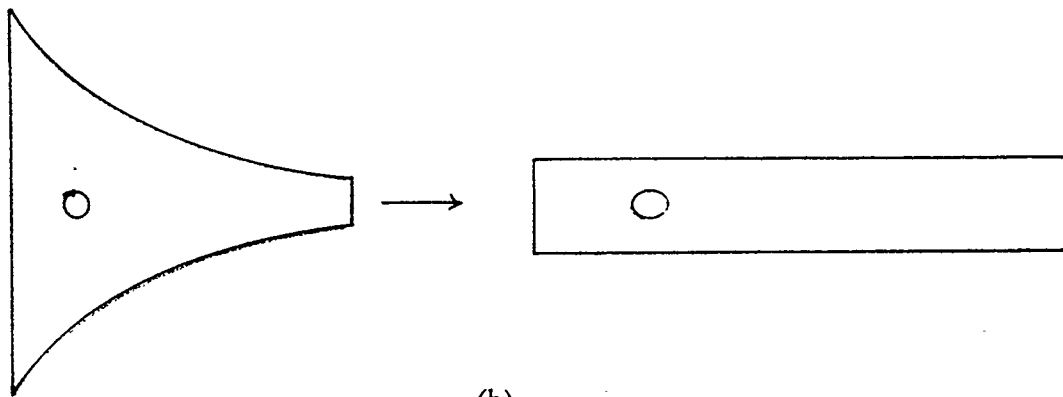
(b)

Figure 5.1:

Flow distortion on transistion from electrode chamber to observation chamber depends on original position

(a)   results in narrow effective stream

(b)   results in broader effective stream

electrode to observation chamber will cause spreading.

The stream diameter is strongly dependent on the concentration of the particles in the sample which is primarily fixed by the required scattering intensity for reliable observations.

5.2. Sample Concentration

Relatively high sample concentrations were used in all instances (greater than 1.6 *% by volume*). This is because during a sample run, the majority of the original sample settles out to the wall of the injection syringe and never enters the test system. In addition, a large number of scatterers are required in order to produce a high enough scattering intensity at the detector for reliable measurement.

5.3. Long Term Stream Stability

During early data runs a slow drift in stream position was observed. For example, two consecutive measurement runs (approximately one half hour each) resulted in 190 μm stream drift for the first run followed by a second run stable to ±12.5 μm.

It has been noted that the worst of these shifts occur approximately simultaneously with ambient temperature shifts (such as air conditioning switching off or recirculation changes within the environment). Forced cooling of the system using a compressed air cannister resulted in deflections in the "positive DEP" direction of 920 μm (see Figure 5.2).
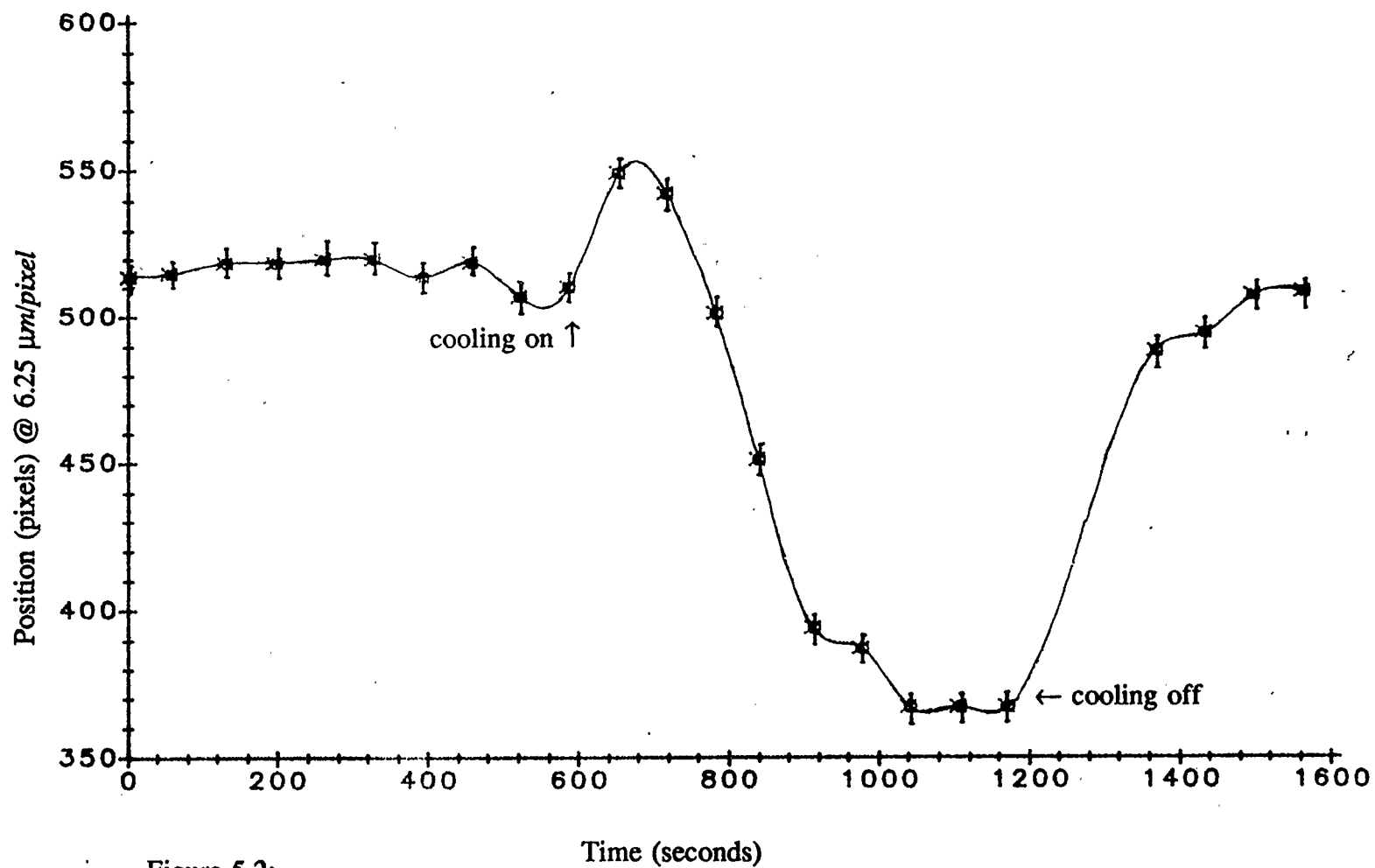
Figure 5.2: Response of stream position to forced cooling of the electrode chamber (no applied field).

It has also been observed that a pocket of warm air forms under the support plate of the pump. This is easily disturbed by small air currents such as those produced by turning the page of a nearby lab book. Subsequent to this observation a small fan was placed to continually prevent the formation of this air pocket. Figure 5.3 illustrates the effect of the fan on stream position.

An insulating jacket (three layers of "Parafilm M" - American Can Co.) around the chamber alone was not found to be sufficient protection, it did however increase the time constant associated with the effect.

The segment-by-segment linearised approximation to the no-field position is subtracted from the stream position read at each point. The resulting figure is used as an estimate of stream displacement at that point. This approach has been used for all measurements in the current work.

5.4. Short Term Stability

In order to obtain an estimate of the error for subsequent measurements, a number of frames were taken with no applied field and the long term drift removed (see the previous section). The estimate of the standard deviation obtained from these measurements is $s < 2.5$ *pixels* or $s < 15.5$ μm. Thus, even though the stream width may be of the order of 150 μm. The location of the stream may be determined to within ± 31 μm ($\pm 5 pixels$) with a 95 % confidence level [38], assuming a normal distribution.
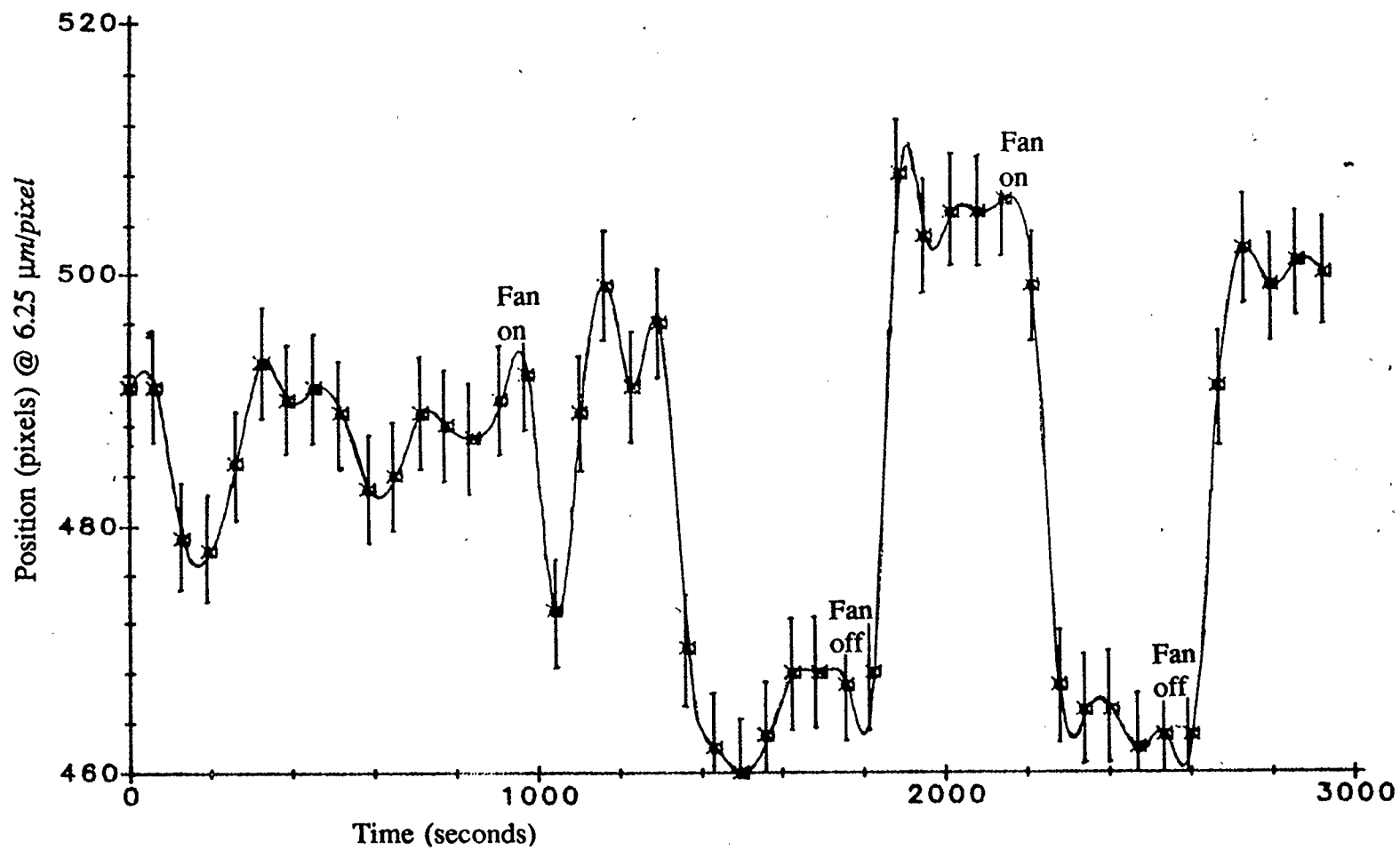
Figure 5.3:

Response of stream position to fan

5.5. V^2 Dependence

Assuming the time spent between the electrodes for any given particle is approximately the same (ie the flow velocity is approximately uniform over the region of displacements considered), the total displacement of the sample stream observed will be proportional to the square of the electrode voltage, other parameters remaining equal.

This hypothesis was tested under various sample conditions and it was found that, depending on the initial sample injection point, the deflection may exhibit a non-linear behaviour beyond a certain magnitude of displacement. It was found that the region of linearity became smaller as the sample injection point was moved into the narrow region of the electrode chamber.

Figures 5.4 illustrate displacement vs V^2 curves for an initial stream position well away from the narrowest region of the electrode chamber. There is no significant non-linearity (<±5 *pixels*) for deflections under 1 *mm* (160 *pixels*).

5.6. Dielectrophoretic Spectrum for Yeast

A number of spectra were obtained for *S. cerivesiae* (yeast) at several suspension conductivities. All of these suffered from poor repeatability.

For the spectrum illustrated in Figure 5.5, three consecutive runs (starting at the high frequencies) were performed, cells for each washed in the same solution of *KCl* ($\sigma = 20$ *μmho/cm*). One would expect that a continuous
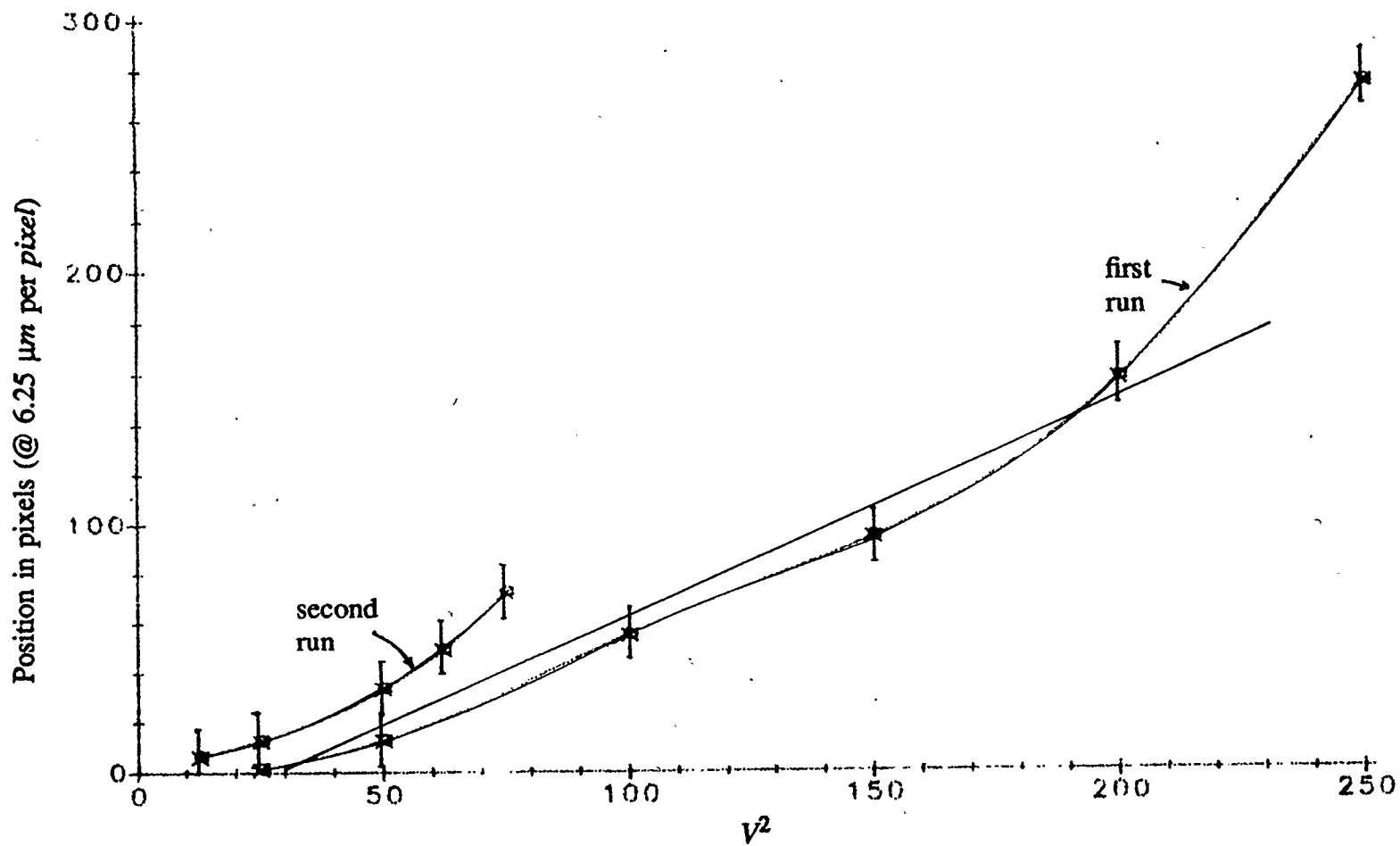
Figure 5.4:

displacement vs. V^2 (linearity) for *S. cerevesiae* at $\sigma = 19.4$ $\mu m/cm$.
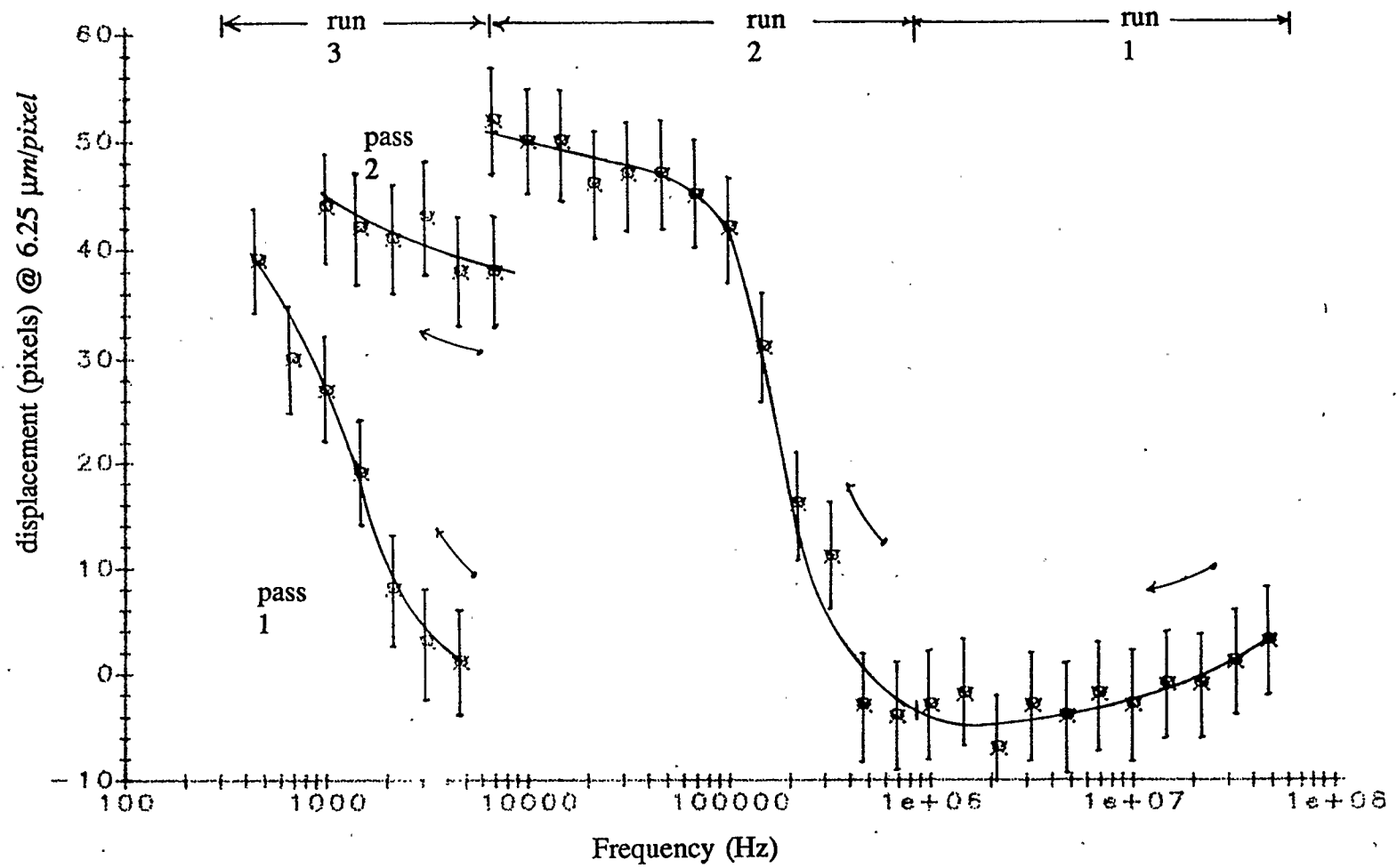
Figure 5.5:

DEP spectrum (*S. cerevesiae*) at $\sigma = 20$ $\mu m/cm$. Note low frequency time dependence.

spectrum would be obtained. As may be seen, a sharp discontinuity is observed between the second and third runs (at 10 *kHz*). In addition, when the range of frequencies below 10 *kHz* is scanned a second time the deflections are significantly different again.

This problem was not observed at high frequencies. For example, the data point at the end of the first run and that at the beginning of the second $(6.81 \times 10^5 \ Hz$ and $4.6 \times 10^5 \ Hz$ respectively) show no major discontinuity.

5.7. Dielectrophoretic Spectrum for Polystyrene-DVB Microspheres

A dielectrophoretic spectrum was obtained for polystyrene-DVB microspheres of $5\mu m$ diameter suspended in 14 *µmho/cm KCl* solution. Peak deflections of up to 36 pixels (225 µ*m*) were recorded and fairly good repeatability observed.

Figure 5.6 illustrates the results of two consecutive runs with the polystyrene-DVB microspheres washed five times in the sheath solution then three more times before the subsequent run. The syringes and chamber system were flushed three times before the first run (⁓ 150 *ml* flushed through the chamber system) to minimise contamination.

Bahaj and Bailey[39] have performed dynamic dielectrophoretic levitation on single DVB microspheres using a ring-disk electrode geometry. Figure 5.7 illustrates a comparison between a DEP spectrum of 5 µ*m* DVB microspheres obtained using the continuous automated DEP system described here and their
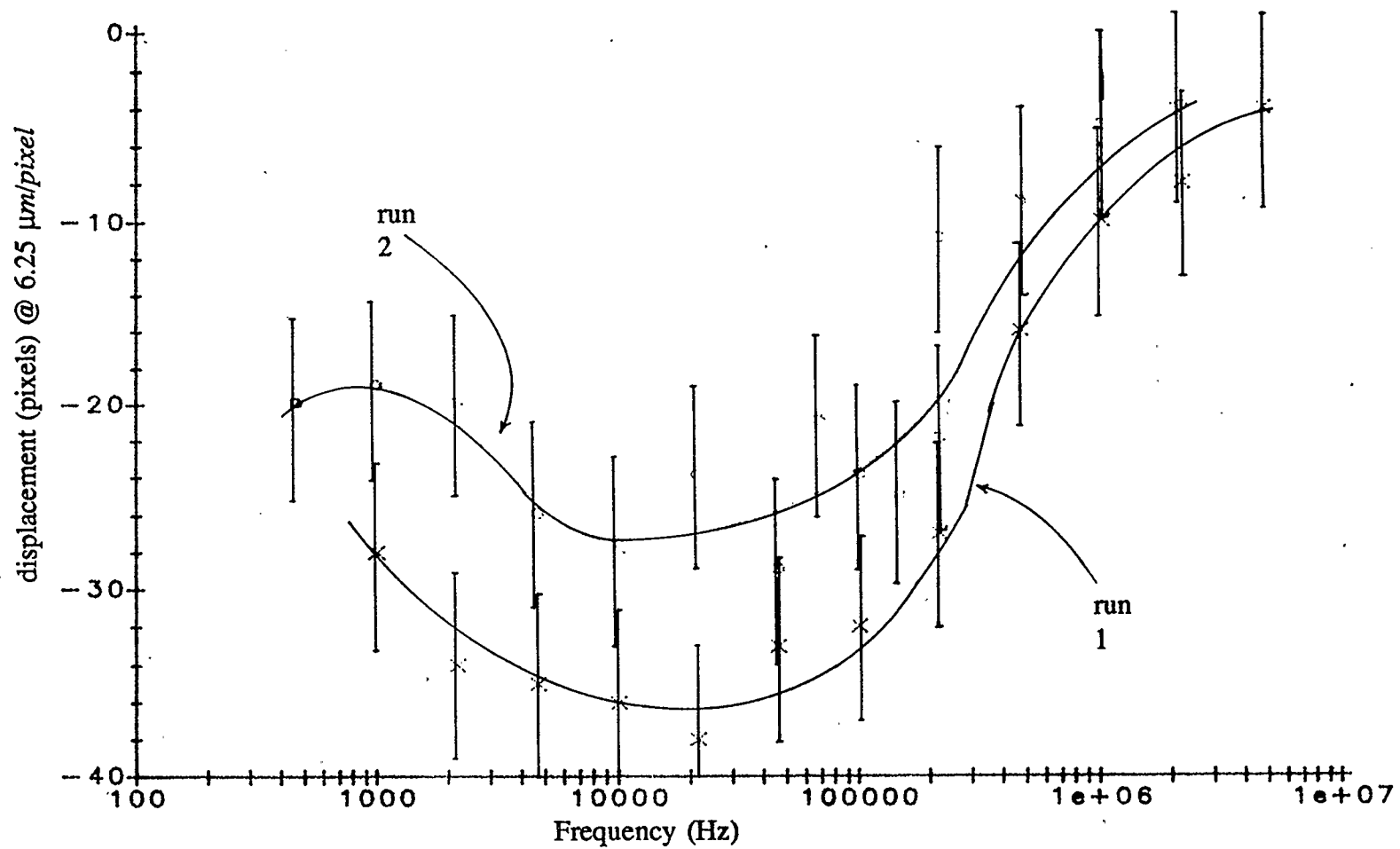
Figure 5.6:

DEP spectrum (polystyrene-DVB 5 μm diameter) at 14 μ *mho/cm*.
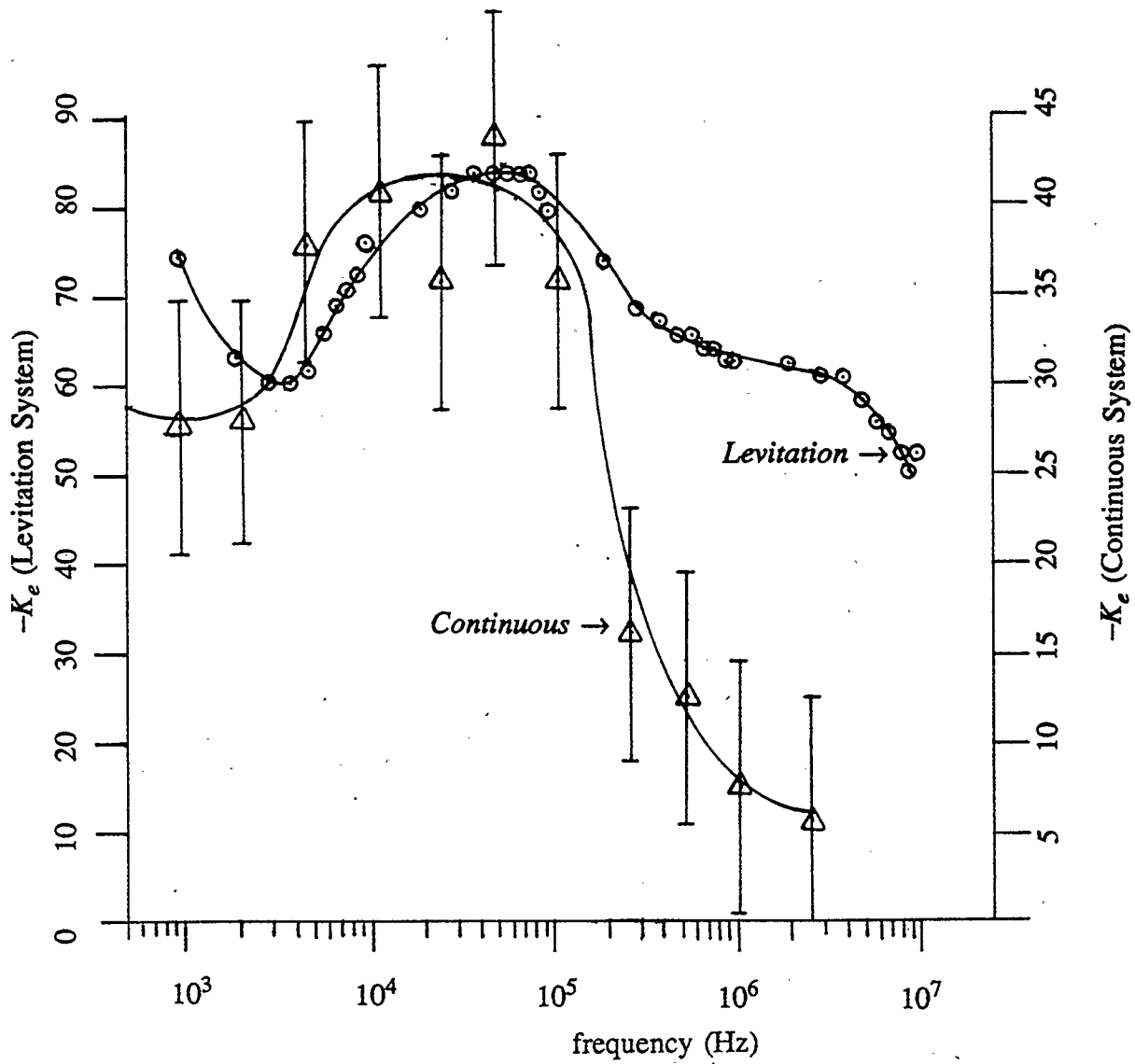
Figure 5.7:

Comparison between single-particle DEP levitation spectrum of 50 μm polystyrene-DVB microspheres in 12 $\mu mho/cm$ KCl solution and a continuous DEP spectrum of 5 μm polystyrene-DVB microspheres in 14.2 $\mu mho/cm$ KCl solution. (Continuous DEP readings taken at 10 V_{pp}.)

results using levitation of 50 μm DVB microspheres.

The calibration of the continuous system is based on a crude estimate (see Section 4.8, and Equation 4.2). There is no mention made as to how the levitation system was calibrated, and the strong position dependence of the DEP force in the ring-disk geometry suggests that calibration would be difficult at best. In light of this, the factor of two difference in absolute magnitude is less important than the observation that the peaks both occur in the same frequency region. It is possible that the discrepancy at high frequency is due to a diameter-dependent relaxation mechanism, such as the ionic effects, which would shift to higher frequency as the diameter of the sample particle is reduced by a factor of ten between the levitation and continuous measurements.

5.8. Effect of Conductivity Mismatch

A number of anomalous results have been observed. These have shown up as a seemingly unrelated family of intermittent anomalies. They include slight stream deflection in one direction before settling to a final deflection in the opposite direction, curved V^2 curves (see Figure 5.8), and deflections opposite the direction predicted (for example negative deflections for yeast in the 5 kHz region, and positive deflections for the microspheres in the same region).

The system consists of a sheath fluid inside which is carried a fluid column within which the sample particles are suspended. These originate from separate syringes (B and A in Figure 4.4). If a mismatch in conductivity or
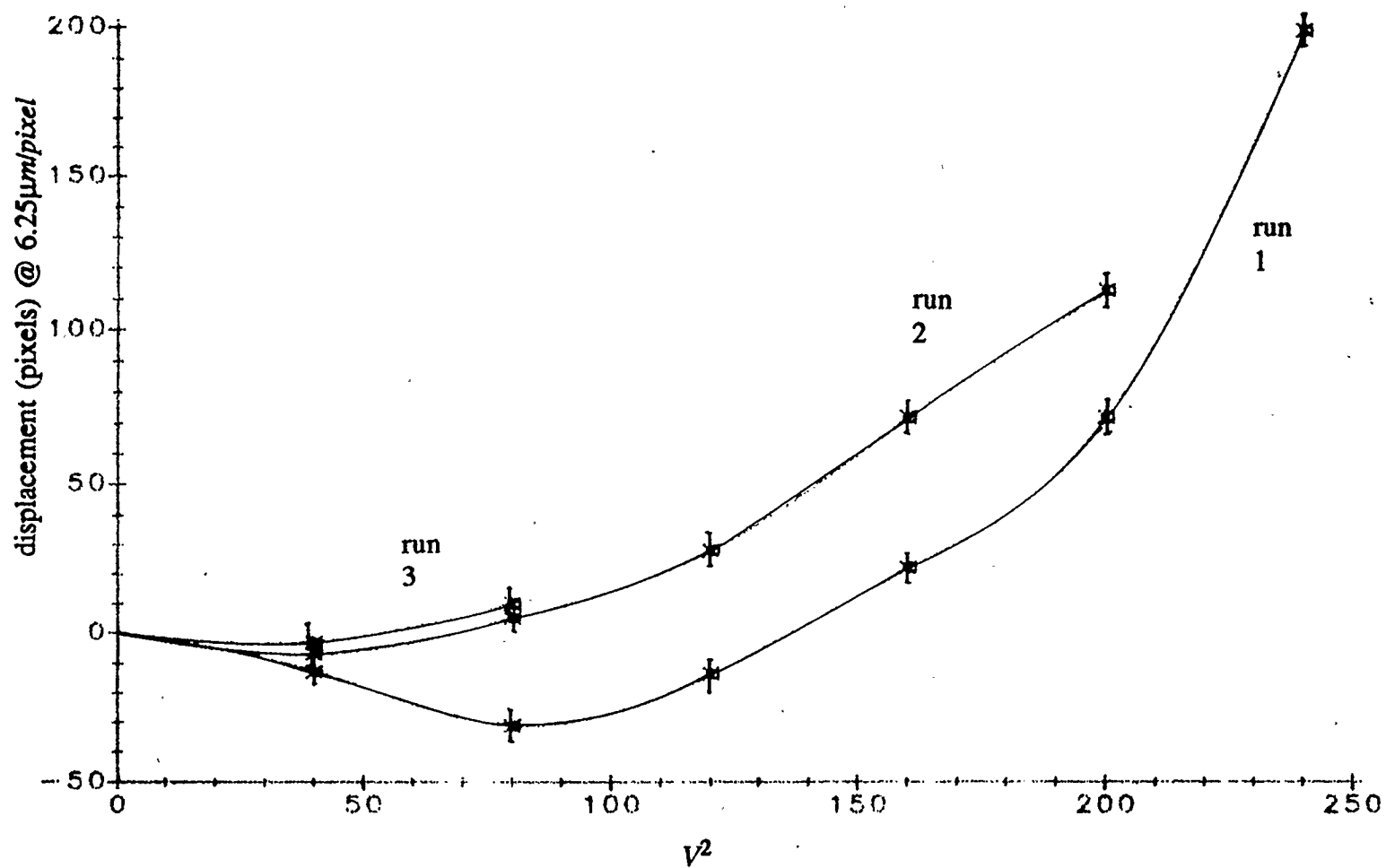
Figure 5.8:

Family of V^2 curves with mismatched fluid conductivities ($\sigma_{sample} < \sigma_{sheath}$).

permittivity occurs between these two fluids then the central *fluid* stream will undergo dielectrophoresis carrying the suspended sample with it. At the same time, the internal particles may undergo DEP in either direction relative to the local fluid. Therefore if the sample suspension fluid conductivity is higher than that of the bulk sheath fluid, a much larger deflection will be observed in the "positive DEP" direction than would be experienced in the ideal case. Similarly, if the sample fluid is of lower conductivity it will undergo negative dielectrophoresis. The effect is illustrated in Figure 5.9.

If the particles are undergoing DEP in the opposite sense to this fluid suspension one may observe a deflection in one direction initially due to the conductivity mismatch, followed by a deflection in the opposing direction provided the field strength is high enough that the particles are drawn clear of the central fluid stream.

This is well illustrated in Figure 5.8 wherein a family of V^2 curves are shown for mismatched fluids. In this case erroneous readings of sample conductivity caused the experimenter to set the surrounding medium to a higher conductivity than that of the sample suspension. As time progresses the yeast cells lose ions osmotically through the cell membrane and wall, increasing the sample suspension conductivity. As a match is approached the negative deflections become smaller and the threshold at which the deflection reversal is observed becomes lower. Note that at low field strength the slope of the curve approaches that representative of the conductivity mismatch between streams, at

$$\nabla \, | \vec{E} |$$

(a)

(b)
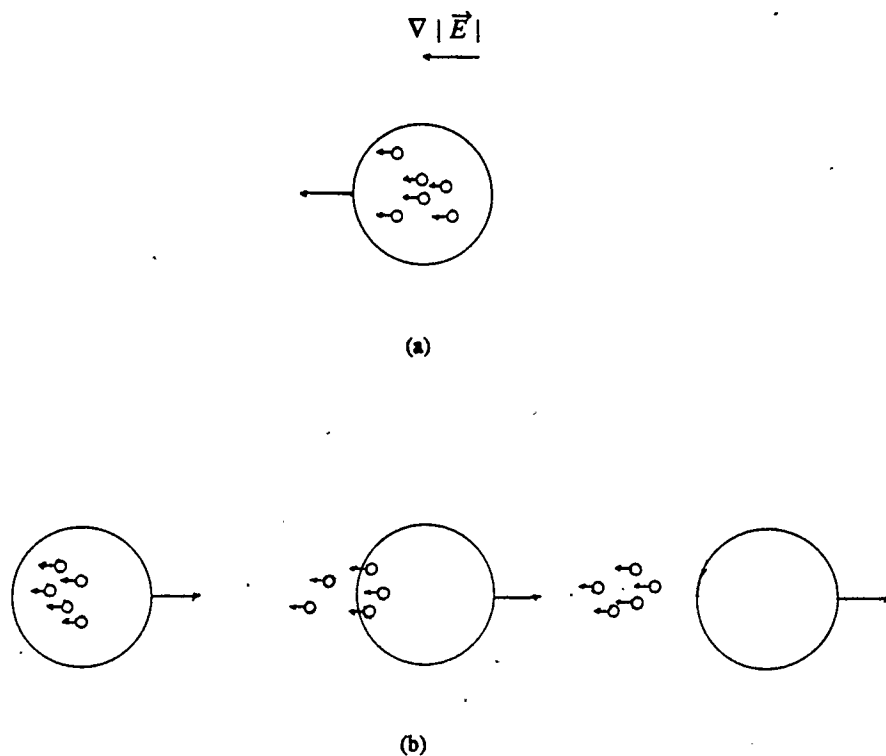
Figure 5.9:

(a) Fluid velocity and particle velocities in same direction: net deflection velocity is the sum of the two.

(b) Fluid velocity and particle velocity in opposite directions: initial deflection is determined by difference between two velocities. If the particles leave the initial sample fluid stream then the final velocity is purely that of the particles.

high field the slope is purely an indication of the effective permittivity of the particles in the sheath fluid and is independent of the initial sample fluid conductivity.

In order to confirm that this is the mechanism behind these anomalies two runs were performed each with a marked mismatch between the fluids in opposite directions. In the first of these the sample was washed and resuspended in water of conductivity 0.65 $\mu mho/cm$ the sheath was KCl solution of conductivity 25 $\mu mho/cm$. Under these conditions the stream becomes very clumpy, even for low fields, indicating a high degree of mutual DEP within the the sample suspension, huge deflections in the "positive DEP" direction were also observed. A clear V^2 curve was not obtained, however, due to extreme field sensitivity, deflections toward the electrodes take place and stream breakup occurs.

In the reverse situation, under high field conditions, the stream tends to swing in the "negative DEP" direction before coming to rest in a final positive position. An example of this is shown in Figure 5.10 for 50 kHz, 20 V_{pp} in which the stream is drawn from a no field position to a field on position of + 49 *pixels* (306 μm) after passing through a transient negative deflection of −35 *pixels* (−219 μm).
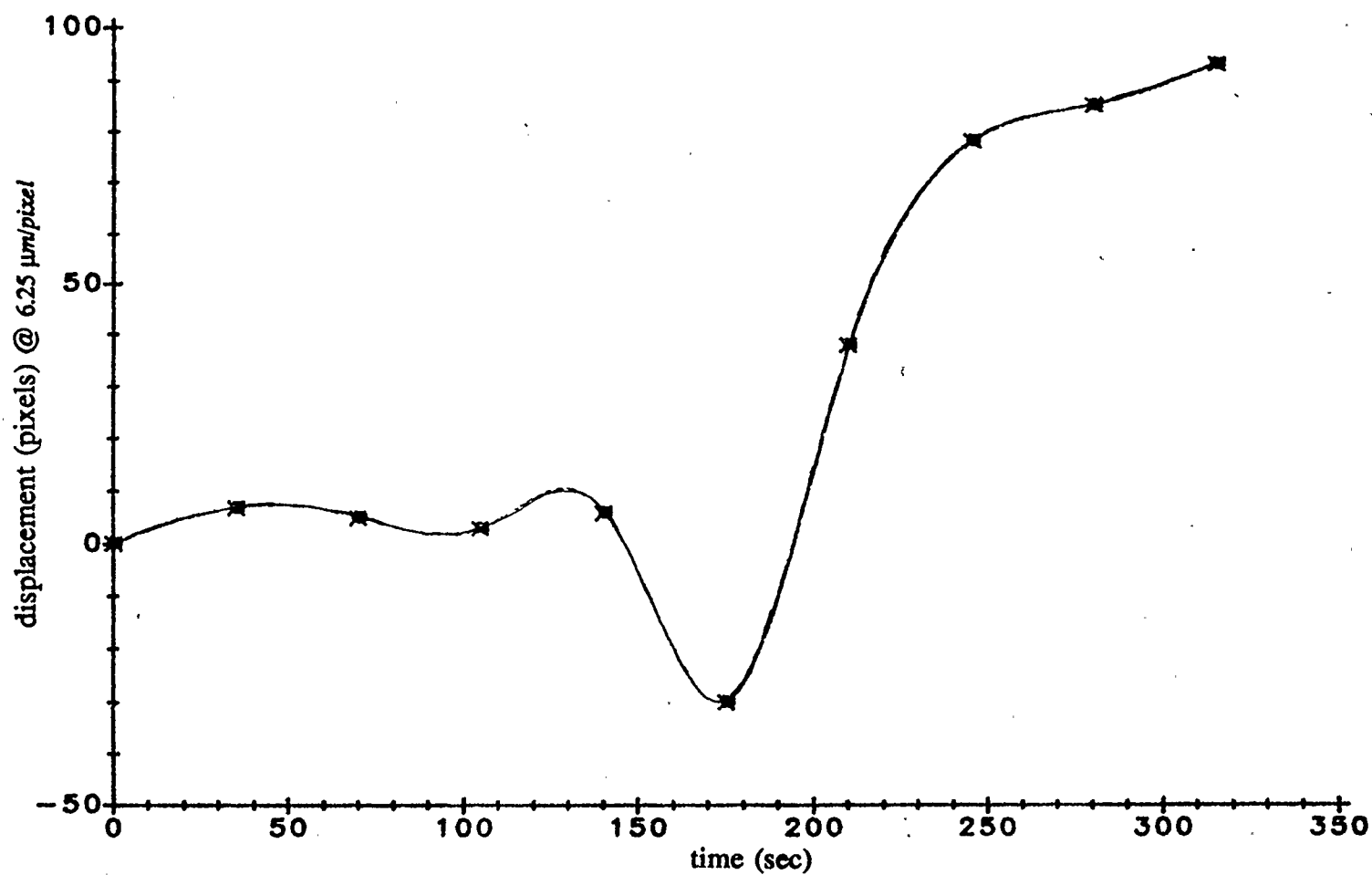
Figure 5.10:

Effect of conductivity mismatch on time response. No field intil 140

seconds then 50 *kHz* @ 20 V_{pp} signal applied. (sample *S. cerevesiae* with

$\sigma_{sample\_fluid} \ll \sigma_{sheath}.$)

CHAPTER 6

CONCLUSIONS and RECOMMENDATIONS

6.1. Summary

A prototype model of a Continuous Automated Dielectrophoretic System has been constructed. This uses the mechanism of dielectrophoresis to deflect a narrow particle stream as it flows between a pair of isomotive electrodes which provide a prescribed field strength and gradient in order that the force is independent of stream position. Deflections are then measured for various applied voltages and frequencies to determine the effective polarisability and polarisability spectra for the sample particles.

The system is **automated** in that the applied voltage and frequency is controlled, and stream width and position acquired, under computer control. It is **continuous** in that a sample is prepared and loaded into a syringe and a stream is made to flow through the electrode chamber for approximately one hour at a time (sixteen to seventeen data points per run) as opposed to earlier batch studies which required loading of sample for each data point.

In addition the sheath fluid is in intimate contact with the electrodes for the length of the electrode chamber allowing lower frequency readings than those obtained in previous continuous systems.

The stream diameters (< 150 µm) and deflections ($\approx$ 1000 µm) achieved with this system are such that it may prove feasible as a separation system. It currently has linear response for a large dynamic range and allows measurement of both positive and negative dielectrophoresis.

Linearity results (deflection vs. V^2) and dielectrophoretic spectra have been obtained.

6.2. Stream Characteristics

The stream appears wider than the target of 50 µm half width originally set. Though usually under 150 µm. This is partially due to the conservative method of estimating the half-width provided by the data acquisition and processing equipment. The positional stability problem may be partially eliminated by taking repeated no-field measurements during the course of a run; however this is not satisfactory in the long term as it wastes five to six data points out of each seventeen to eighteen point data run. Were the stream stable over the course of a run this could be reduced to one or two data points.

These two problems are not expected to represent fundamental limitations on the usefulness of the instrument. Further refinement of the injecter may produce slightly narrower stream widths. However it has been observed over a number of attempts that the 125 µm to 175 µm range of stream diameters is the best attainable consistently. A more promising avenue to explore would be the effect of further increasing the ratio of sheath syringe barrel diameter to that of

the sample syringe. This would serve to reduce the sample flow rate with respect to the sheath flow rate at the injection point providing a better "necking" effect. Stream diameters of 80 μm to 90 μm have been observed when injecting in higher flow-rate regions of the chamber, unfortunately the stream in the electrode chamber then nears an area of non-linear response due to the field gradients near the origin of the isomotive geometry (see Figure 3.4). This result may have been influenced by the flow distortion at the electrode-observation chamber transition (see Figure 5.1). This does, however, suggest that the higher ratio of flow rates may produce narrower streams.

The thermal stability performance is not well understood and hence a thermal control system (such as an environmental chamber or a circulating water bath system) should be incorporated in order to identify the thermal sensitivity of the components and how best to control the problem. A thermal control feature incorporated into the system may lend itself to potentially fruitful studies of thermal effects on DEP spectra of various particles of biological origin (see below).

6.3. Sample Concentration

Because the sample tends to settle out within the sample syringe during the course of a run, the absolute sample concentration need only be held within a very broad range. The low end of the range is approximately 1500 *particles/ml* However, as the concentration increases there is no clearly

defined upper limit. Signal strength increases with concentration and, eventually, the width increases as well. This point is not well defined and is dependent on the tendency of the sample particles to clump.

It is desirable to avoid the settling of particles in the sample syringe as some biological particles tend to clump resulting in erratic flow as the clumps pass through the injecter. In addition to this, the time varying nature of the signal strength, which is currently experienced as the sample particles settle out is also undesirable. Alternative sample containment and drive schemes may be worth investigating in order to incorporate sample suspension agitation.

6.4. Linearity

The V^2 curves obtained (eg Figure 5.4) suggest that there is a good linear relationship between the square of the applied voltage and the displacement in stream position within limited deflection ranges. The linear range is dependent on the point at which the stream is injected, as the flow profile (Figure 4.6) is non-uniform. For certain regions of the stream good linearity may be obtained for deflections up to 1 *mm*. This probably corresponds to areas of near-uniform flow velocity. As greater deflections are observed in the "positive DEP" direction (into the region of higher field intensity) a characteristic up-turn occurs at the top end of the curve. This is because the stream is moving into a lower flow velocity region of the chamber and thus is spending a greater period of time between the electrodes than it does when in the low-field positions

(where the chamber is broadest). This results in a greater net deflection than is predicted by the uniform-flow-velocity model of the system.

In order to obtain quantitative results, correlating the observed deflections with a value for the effective permittivity (K_e), it is crucial to obtain the flow rates in the area about the stream. In addition, the non-linear top-end of the V^2 curve may potentially be calibrated out if a thorough understanding of the flow profile is obtained and the measured stream position related to corresponding flow velocities.

6.5. Dielectrophoretic Spectra

Preliminary spectra were obtained for polystrene microspheres and, with moderate success, yeast. The discovery of the extreme sensitivity of the system to conductivity mismatches between the two fluids (sample suspension and sheath solution) offers the single greatest difficulty in operation of the system. It has been shown, in the case of DVB microspheres, that with a great deal of attention to cleansing procedures and matching of conductivities reasonably repeatable results may be obtained over a wide frequency range. The difficulty in obtaining as positive a result from the living samples stems from the harshness of the environment to which they are exposed and their subsequent loss of ions to the sample solution.

Investigation into the effects of isotonic solutions (eg sorbitol) is to be undertaken immediately as the replacement of the $K\ Cl$ solution with a buffer

should effectively limit if not eliminate the ion-loss problem. Thus allowing much more consistent conductivity matches to be obtained. A further modification to the system should incorporate continuous monitoring of both the sample and sheath fluid conductivities.

6.6. Recommendations for Further Work

The system currently is of use as an experimental tool for measuring the DEP response of a variety of particles. In addition to the refinements mentioned above it is of primary importance to investigate the potential of this instrument as a separator of mixed populations. This is ultimately where the greatest potential of the instrument lies as a laboratory tool. A preliminary study in which two widely differing particle populations, such as polystyrene-DVB microspheres and *S. cerevisiae*, are passed through the system under field conditions in which they would deflect in opposite directions, should produce a double stream. If this is undertaken and a positive result obtained then the principle of a continuous DEP separator is proven. It then remains only to construct a stream division system which would allow recovery of the separated populations to produce a useful separator and to test its efficiency.

Performance of the system as a characterisation tool would be enhanced by modification to allow the use of laser doppler velocimetry to monitor deflection velocities directly near the top of the electrode chamber. This is both faster and more exact as the translation velocity is independent of both

the flow velocity (eliminating the effect of non-uniform flow profile) and of the distortion of flow cross-section which the system now suffers from in flow transition from the isomotive electrode chamber to the rectangular observation chamber.

The observation chamber cross section should be modified to better approximate that of the isomotive electrode chamber. Careful consideration must be given, however, to the optical distortion incurred with non-flat-walled chambers.

If recommendations of environmental temperature control testing (mentioned above) are to be followed it would be interesting to investigate the effects of temperature on a wide variety of particles, biological and otherwise. Biological membranes, when isolated from the living state, are known to undergo significant structural changes between 4C and 37C [40]. This area of investigation may provide insight into the (as yet unknown) mechanisms by which living cells inhibit fluid-crystaline transitions of membranes [40].

Greater signal strength and more rapid readings through shorter averaging times may be attained by the use of a more powerful laser light source. This would require greater care in construction and alignment of the observation chamber to minimise stray scattering which may interfere with the desired image at the detector.

Preliminary investigation into the system as a particle separator is currently under way.

6.7. Conclusions

The development of an instrument such as the Continuous Automated Dielectrophoretic System is a major task requiring many man-years to translate the concept into a viable laboratory instrument suitable for day-to-day operation. The portion of the task undertaken here was to develop a basic prototype instrument incorporating several refinements over previous systems. This is to be further refined as knowledge of critical operating parameters and procedures becomes better defined.

A number of observations have led to greater understanding of the operation of the instrument. These include the effect of non-uniform flow velocity profile superimposing an effective non-linearity on the system which may otherwise be linear; and the extreme sensitivity of the system to conductivity mismatches between sample suspension and sheath fluid. The system appears also to be temperature sensitive. However this has not yet been quantified.

There are a wide variety of physical mechanisms which can affect the polarisation characteristics of particles (see Chapter 3). In the case of biological systems, these are most often associated with the membranes. The system described here represents a prototype of a novel tool with which to investigate the surface properties of particles.

The system is presently in need of further refinements before its ultimate limits as a characterisation instrument may be determined. In addition, its potential in separation applications has yet to be fully defined.

The future potential investigations using this instrument are extremely varied. The combination of dielectrophoretic studies with chemical or electromagnetic treatment of cells offers an opportunity to correlate known changes in surface properties with changes in DEP spectra. The measurement of changes in DEP spectra with thermally induced phase changes within isolated membranes (vesicles) (as has been suggested earlier) would allow the investigation of physical mechanisms within the membrane which contribute to polarisation characteristics.

The system currently holds great potential as a tool for biophysical research, however the ultimate sensitivity and flexibility as both a measurement device and a separator have yet to be determined.

BIBLIOGRAPHY

1. H.A. Pohl, *Dielectrophoresis : The Behaviour of Neutral Matter in Nonuniform Electric Fields,* Cambridge University Press, Cambridge (1978).

2. K.K. Kumar and W.J. Lykke, "Cell Separation: A Review," *Pathology* **16** pp. 53-62 (1984).

3. D.B. Milne, N.V.C. Ralston, and J.C. Wallwork, "Zinc content of cellular components of blood: Methods of cell separation and analysis evaluated.," *Clinical Chemistry* **31**(1) pp. 61-69 (1985).

4. T. de Witte, E. Koeckman, E. Geestman, A. Plas, G. Blankenboorg, J. Wessels, and C. Haanen, "Separation of immunoreactive lymphocytes from pluripotent stem cells (CFR-GEMM) by means of counterflow centrifugation.," *Blut* **48** pp. 139-145 (1984).

5. T. de Witte, A. Plas, E. Koeckman, G. Blankenboorg, M. Salden, J. Wessels, and C. Haanen, "Cell size monitored counterflow centrifugation of human bone marrow resulting in clonogenic cell fractions substantially depleted of small lymphocytes.," *J. Immun. Meth.* **65** pp. 171-182 (1983).

6. A. Tulp, A. Timmerman, and M.G. Barnhoorn, "A separation chamber to sort cells and cell organelles by weak physical forces. III Preparative electrophoresis of cells in stationary density gradients at low electric field strength," *Anal. Biochem.* **124** pp. 432-439 (1982).

7. A. Tulp and M.G. Barnhoorn, "A separation chamber to sort cells and cell organelles by weak physical forces. V A sector-shaped chamber and its application to the separation of peripheral blood cells.," *J. Immun. Meth.* **69** pp. 281-195 (1984).

8. A. Tulp, J.A. Aten, M.G. Barnhoorn, W.P. van Beek, J.G. Collard, R. Lutter, and J.G. Westra, "Separation of cells and cell organelles by weak physical forces. IV Applications," *Cell Function and Differentiation* **Part A** pp. 105-114 (1982).

9. S.B. Miller, G. Saccomani, T.P. Pretlow, P.M. Kimball, J.A. Scott, G. Sachs, and T.G. Pretlow II, "Purification of cells from livers of carcinogen-treated rats by free-flow electrophoresis.," *Cancer Research* **43** pp. 4176-4179 (1983).

10. H. Walter and E.J. Krob, "Surface differences between erythrocytes from arbitrarily chosen (presumably hematologically normal) individuals detected by cell partitioning.," *Biochem. & Biophys. Res. Com.* **120**(1) pp. 250-255 (1984).

11. V. Matsumoto, V.M. Ban, and Y. Shibusawa, "Surface affinity chromatographic separation of blood cells. IV Relationship between surface hydrophobicity of human peripheral blood cells and their retention behaviour on polyethylene glycol 20M-bonded sepharose columns.," *J. Chromatogr.*, pp. 389-399 (1984).

12. H.W. Tyrer, "Instrumentation for analyzing biological cells.," *IEEE Potentials*, pp. 20-24 (December 1984).

13. R. Pethig, *Dielectric and Electronic Properties of Biological Materials*, John Wiley & Sons, Chichester (1979).

14. H.A. Pohl, Karan Kaler, and Kent Pollock, "The Continuous Positive and Negative Dielectrophoresis of Microorganisms"," Research Note, Quantum Theoretical Research Group, Oklahoma State University, Stillwater 74074 (June 1978).

15. A.A. Teixeira-Pinto, L.L. Nejelski Jr., J.L. Cutler, and J.H. Heller &T The Behaviour of Unicellular Organisms in and Electromagnetic Field, *Experimental Cell Research* **20** pp. 548-564 (1960).

16. H.A. Pohl and I. Hawk, *Science* **152** p. 647 (1966). after Pohl (1978)

17. U. Zimmermann, "Electric Field-Mediated Fusion and Related Electrical Phenomena," *Biochimica et Biophysica Acta* **694** pp. 227-277 (1982).

18. C.S. Chen and H.A. Pohl, *Ann. N.Y. Acad. Sci.* **238** p. 176 (1974).

19. Karan Kaler and Herbert A. Pohl, "Dynamic Dielectrophoretic Levitation of Living Individual Cells," *IEEE Transactions on Industry Applications* **1A-19**(6)(Nov./Dec. 1983).

20. B.D. Mason and P.M. Townsley, *Can. J. Microbiol.* **17** p. 879 (1971).

21. K.V.I.S. Kaler, O.G. Fritz Jr., and R.J. Adamson, "Quasi-elastic light scattering studies on yeast cells undergoing dielectrophoresis.," *IEEE Trans. Ind. Appl.* **IA-22**(1)(1986).

22. H.P. Schwan, "Biophysics of the Interaction of Electromagnetic Energy with Cells and Membranes," *NATO Advanced Study Institutes Series: Biological Effects and Dosimetry of Nonionizing Radiation* A **49** pp. 213-231 (1981).

23. H.P. Schwan, "Electrical Properties of Cells: Principles, Some Recent Results, and Some Unresolved Problems.," in *The Biophysical Approach to Excitable Systems.*, ed. D.E. Goldman, Plenum Pub. Corp., New York, N.Y. (1981).

24. E.H. Grant, R.J. Sheppard, and G.P. South, *Dielectric Behaviour of Biological Molecules in Solution,* Clarendon Press (Oxford University Press), Oxford (1978).

25. R.J. Adamson and K.V.I.S. Kaler, "Multipole effects on the dielectrophoretic force in an 'isomotive' field," *J. Biological Physics* **13** pp. 95-98 (1985).

26. T.B. Jones and G.A. Kallio, "Dielectrophoretic Levitation of Spheres and Shells," *J.Electrostatics* **6** pp. 297-224 (1979).

27. H.A. Pohl and Kent Pollock, "Electrode Geometries for Various Dielectrophoretic Force Laws," Research Note, Quantum Theoretical Research Group, Oklahoma State University, Stillwater 74074 (Sept. 1977).

28. Arthur von Hippel, "Theory," in *Dielectric Materials and Applications,* ed. A. von Hippel, The Technology Press of M.I.T. and John Wiley and Sons, New York, N.Y. (1954).

29. S.S. Dukhin and V.N. Shilov, *Dielectric Phenomena and the Double Layer in Disperse Systems and Polyelectrolytes,* Halsted Press (1974). translated from Russian.

30. J.C. Maxwell, *A Treatise on Electricity and Magnetism,* Clarendon Press, Oxford (1881). in Dukhin and Shilov

31. K.W. Wagner, *Die Isolierstoffe der Elektrotechnik,* Springer, Berlin (1924).

32. H.P. Schwan, "Electrical Properties of Tissue and Cell Suspensions," *Advances in Biological and Medical Physics* **5** pp. 147-209 (1957).

33. J.A. Stratton, *Electromagnetic Theory,* McGraw-Hill, Inc., New York (1941).

34. Gerhard Schwarz, "A Theory of the Low-Frequency Dielectric Dispersion of Colloidal Particles in Electrolyte Solution," *J. Phys. Chem.* **66** pp. 2636-2646 (1962).

35. T.J. Lewis, *The Dielectric Behaviour of Non-Crystaline Solids,* (personal communication with Dr. K.V.I.S. Kaler) 1977.

36. Vera V. Daniel, *Dielectric Relaxation,* Academic Press, London (1967).

37. John Happel and Howard Brenner, *Low Reynolds Number Hydrodynamics with Special Applications to Particulate Media,* Prentice-Hall, Inc., Englewood Cliffs, N.J. (1965).

38. Herbert L. Anderson (ed. in chief), *AIP 50th Anniversary Physics Vade Mecum ,* American Institute of Physics, New York, NY (1981).

39. Abubakr S. Bahaj and Adrian G. Bailey, "The Relationship Between Dielectrophoretic and Impedence Response of Dielectric Particles Immersed in Aqueous Media," *IEEE Transacions on Industry*

Applications **IA-21**(5) pp. 1300-1305 (Sept/Oct 1985).

40. Micheal McCloskey and Mu-ming Poo, "Protein Diffusion in Cell Membranes: Some Biological Implications," *Int. Rev. of Cytology* **87** pp. 19-81 (1984).

APPENDIX A

Software Description and Operation

The HP 9816 desk-top computer running the BASIC 3.0 operating system is used to control and initialise the signal generator (Wavetek 178) and data acquisition processor (Data Precision: Data 6000), and to collect results from the latter. This is accomplished via an IEEE 488 instrument control bus.

Although software has been written to perform a large number of functions, including exchange of data between disks and the Data 6000, it was found that very few functions were actually used during the testing of the system. (Reasons for this stem primarily from the low transfer rates attainable to and from the Data 6000 due to the protocol that this instrument demands and the lack of on-board processing power.)

The final program, DEP_MIN, is a minimal version of the original software package and has only two levels of menu. Figure A.1 illustrates the hierarchy of the system. The MAIN MENU is obtained by running a program entitled DEP_MIN. Time/Date (a function) and Auto-Run are selections from that menu. Auto-Run produces a further menu with ten possible selections, each being a function.
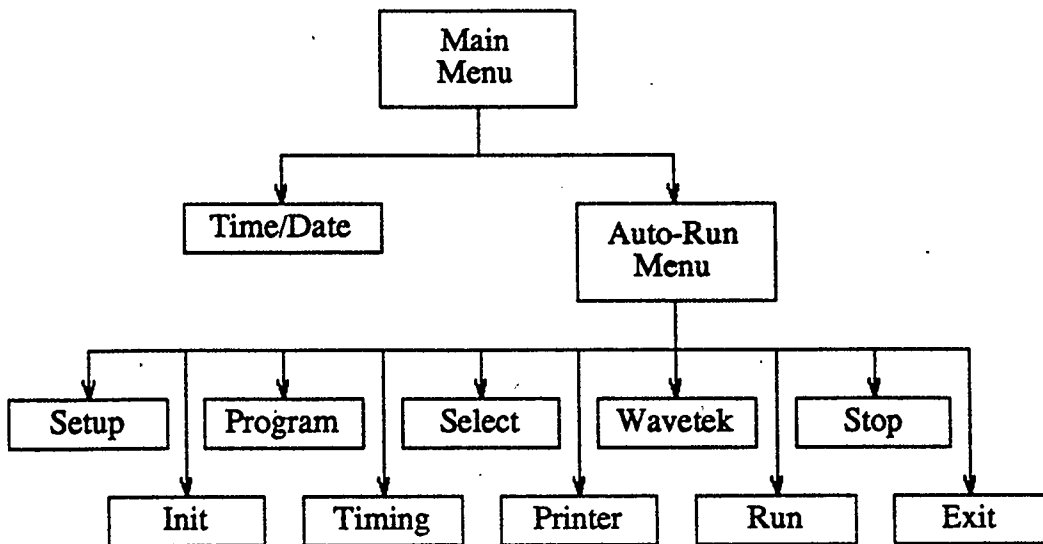
Figure A.1: "DEP_MIN" command heirarchy.

1. Functions

Time/Date

- allows initialisation of internal clock to current date and time

- called only once each time the computer is powered on.

Init

- initialises interfaces for the instruments on the IEEE 488 bus

- may only be called once each time the system [RESET] function is activated or after power on.

Setup

- down-loads initial display and program information to the Data 6000

- initialises the signal source to switch output off.

Prog

- allows modification of the data processing program or setup of the Data 6000 by typing commands directly

- allows initialisation of the "BACK" background data frame

- exited with "." at the left hand column.

Timing

- set period with which Data 6000 is to be queried for results (eg. if 128 averages are used then the Data 6000 may be queried as often as every 35 seconds)

- allows selection of an audible count of the number of samples acquired since the last time the field was modified.

Select

- The four variables for which the user is prompted will be the variables the Data 6000 is queried for (they may also be any Data 6000 command with a single valued result)

- the same variable (or command) will be placed at the head of the appropriate column of the printout

- the values corresponding to these variables will be logged with a period selected by the [Timing] function.

Hardcopy

- selecting this function toggles the output from the printer to the screen (default: Hardcopy off)

- the resulting status is displayed (eg. "Hardcopy ON")

Wavetek

- prompts for amplitude (volts peak to peak) and frequency (in Hz)

- [ENTER] as a response leaves previous value unchanged

- may use FORTRAN notation (eg. a frequency of "10.0e6" interpreted as 1 MHz)

Run

- start periodic logging of data

- performs page eject (or clear screen if Hardcopy OFF).

Stop

- stop logging data

Exit

- exit to main menu

-

Note: if |Exit| followed by |Auto-Run| then |Setup| and |Select| must both be re-executed as the resulting variables have been un-initialised.

APPENDIX B

Sample Data Log

The HP9816 desk top computer logs the command sequence sent to the Data 6000 during initialisation. The header of each page contains the date and current time. An example follows of the complete log including setup.

Data 6000 Initialisation

NPTS=1024	1024 samples per scan
PERSRC=3	synchronously sampled data
TRGSRC=7	external trigger (from end-of-line)
TRGLEV=2	trigger level = 2 V
TRGM=1	normal triggering
INPSEL=2	select input number 2 and ...
REC=1	... disable it
INPSEL=3	select input number 3 and ...
REC=1	... disable it
INPSEL=4	select input number 4 and ...
REC=1	... disable it
INPSEL=1	select input number 1
AVGCNT=256	default to 256 scan averaging
AVGM=2	continuous averaging

EXECON=1	execute only on run/stop command
DSPM=2	display 2 traces
XSTART=384	beginning of cursor at pixel 384
XDELTA=256	cursor length=256 pixels
CURSOR=2	turn cursor on
BLINE=2	turn baseline on
XOFF(1)=512	horizontal offset on trace 1
XOFF(2)=512	horizontal offset on trace 2
CNVINP=1	internal convolution window
CNVNPT=10	ten point window for convolution
CNVOFF=-5	five point offset centres window
CONVM=1	zero fill outside window region
CNVWDW=2	triangular convolution window
	Beginning of program:
10 SUB.A1=BACK-AVG.A1	subtract averaged signal from background
20 CONVA1=CONV(SUB.A1)	convolve result with window
30 WIDTH=CR:PLSW(CONVA1)	calculate stream width
40 BLEVEL=CR:MAX(CONVA1)	set baseline to peak level of CONVA1
50 LOC=CR:BL:CRS(CONVA1)	find point where CONVA1 crosses baseline
60 TRLOC=TRND(LOC,,512,0,0)	plot a trend of the peak location
70 PK.PK=CR:PK.PK(CONVA1)	determine peak-to-peak signal amplitude

Data Log

The data log is divided up into up to six columns. the first two columns are fixed to be the sample count, the number of times the system has been queried since the beginning of the run, and the time of the sample acquisition. The remaining four columns contain the data selected by the user. The head of each column identifies the contents as "SAMPLE", "TIME", and the command used to query the Data 6000.

The usual parameters queried are: LOC (stream location in pixels); WIDTH (stream width in pixels); and PK.PK (peak to peak signal amplitude in volts) - the last column is not used.

The above pattern is broken whenever the user requests a field change of the signal generator at which time a single line is printed containing: the current time; "Frequency = " followed by the requested frequency setting; and "Amplitude = " followed by the requested amplitude. If an amplitude of zero is requested then the time and "No Field" is printed.

SAMPLE	TIME	LOC	WIDTH	PK.PK
1	21:05:29	658	3	0.0082717
2	21:06:04	530	12	0.0094899
3	21:06:39	477	20	0.065126
4	21:07:14	469	19	0.2173
5	21:07:49	466	20	0.22074
6	21:08:24	466	22	0.23242
7	21:08:59	465	17	0.23307
8	21:09:34	461	24	0.247
9	21:10:09	470	17	0.27696
10	21:10:44	467	23	0.21149
11	21:11:19	473	20	0.32263
12	21:11:54	465	32	0.34748
21:12:14	Frequency	= 1.00E4 Hz		Amplitude = 14.1 Vpp
13	21:12:29	471	23	0.61851
14	21:13:04	485	51	0.3867
15	21:13:39	492	46	0.40712
16	21:14:14	477	31	0.43186
17	21:14:49	476	30	0.42037
18	21:15:24	478	29	0.47161
21:15:29	Frequency	= 1.00E4 Hz		Amplitude = 17.32 Vpp
19	21:15:59	477	28	0.47215
20	21:16:34	463	49	0.1803
21	21:17:09	475	41	0.089423
22	21:17:44	476	38	0.07497
23	21:18:19	480	33	0.083157
21:18:29	Frequency	= 1.00E4 Hz		Amplitude = 20 Vpp
24	21:18:54	477	33	0.090469
25	21:19:29	479	33	0.047994
26	21:20:04	493	31	0.024195
27	21:20:39	516	25	0.23143
28	21:21:14	516	24	0.37737
21:21:20	Field OFF			
29	21:21:49	525	25	0.35539
30	21:22:24	483	47	0.52457
31	21:22:59	461	15	0.036784
32	21:23:34	470	20	1.01
33	21:24:09	466	19	1.0661
21:24:14	Frequency	= 1.00E4 Hz		Amplitude = 20 Vpp
34	21:24:44	469	24	0.75216
35	21:25:19	545	76	0.28669
36	21:25:54	449	51	0.26311
37	21:26:29	516	28	0.2058
38	21:27:04	539	30	0.2139
21:27:11	Frequency	= 1.00E4 Hz		Amplitude = 17.32 Vpp
39	21:27:39	538	28	0.27353
40	21:28:14	513	35	0.27272
41	21:28:49	474	24	1.3036
42	21:29:24	476	24	1.1862
43	21:29:59	472	19	1.1367
21:30:03	Frequency	= 1.00E4 Hz		Amplitude = 14.14 Vpp
44	21:30:34	472	25	0.90819

SAMPLE	TIME	LOC	WIDTH	PK.PK
45	21:31:10	465	23	1.217
46	21:31:44	479	20	1.079
47	21:32:19	479	20	0.96993
48	21:32:54	478	19	1.002
21:32:55	Field OFF			
49	21:33:29	474	21	0.9889
50	21:34:04	461	18	0.63754
51	21:34:39	461	18	0.86134
52	21:35:14	460	22	0.89244
53	21:35:49	461	22	0.81572
21:35:56	Frequency	= 1.00E4 Hz		Amplitude = 10 Vpp
54	21:36:24	462	18	1.037
55	21:36:59	493	30	0.66532
56	21:37:34	485	21	0.94772
57	21:38:09	482	24	0.7991
58	21:38:44	484	19	0.87844
21:38:53	Frequency	= 1.00E4 Hz		Amplitude = 20 Vpp
59	21:39:19	486	25	0.75813
60	21:39:54	481	39	0.16423
61	21:40:29	498	24	0.071732
62	21:41:04	526	34	0.15859
63	21:41:39	560	21	0.19009
64	21:42:14	560	21	0.20454
21:42:20	Frequency	= 1.00E4 Hz		Amplitude = 18.7 Vpp
65	21:42:49	550	28	0.21449
66	21:43:24	522	34	0.12844
67	21:43:59	506	26	0.26307
68	21:44:34	511	23	0.23154
69	21:45:09	504	24	0.22506
70	21:45:44	504	24	0.20638
21:45:54	Frequency	= 1.00E4 Hz		Amplitude = 17.32 Vpp
71	21:46:19	509	24	0.17655
72	21:46:54	504	29	0.22138
73	21:47:29	487	26	0.37514
74	21:48:04	484	25	0.5405
75	21:48:39	488	21	0.67666
21:48:45	Frequency	= 1.00E4 Hz		Amplitude = 19.36 Vpp
76	21:49:14	478	27	0.47662
77	21:49:49	483	35	0.27667
78	21:50:24	528	26	0.18119
79	21:50:59	532	19	0.20091
80	21:51:34	530	24	0.15266
21:51:38	Frequency	= 1.00E4 Hz		Amplitude = 18.03 Vpp
81	21:52:09	546	26	0.11875
82	21:52:44	522	35	0.12582
83	21:53:19	512	27	0.14257
84	21:53:54	507	23	0.2001
85	21:54:29	509	21	0.25421
21:54:35	Field OFF			
86	21:55:04	504	25	0.19778
87	21:55:39	478	37	0.37292

APPENDIX C

Fluid System Operation

1. Priming the System

To start, the effluent flask (O in Figure 4.4) is filled with clean, filtered, distilled water. The drain tube is immersed and the "outlet" valve (F) opened. The sample and medium syringes are both partially filled with clean water and the "inlet" valve (E) closed. The bleeder syringe is empty and its valve (D) opened. The fluid is drawn from the effluent flask into the observation chamber using **gentle** pressure on the bleeder syringe. After this, the flow must be **slowed** by using the same syringe as the syphon effect takes over. By observing the electrode chamber through the clear plexiglass the formation of closed air pockets is prevented by slowing the rate at which air is displaced into the bleeder syringe until the surface level of the fluid equalises before proceeding. The level, in some cases, must be allowed to rise and fall about the level at which a bubble tends to form.

When the chamber is filled to the level of the bleeder port (H in Figure 4.4) the "outlet" valve (F) is closed and "inlet" valve (E) opened. When the syringe pump is turned on fluid is forced through the medium and sample inlets, displacing trapped air into the chamber. This is trapped at the bleeder

outlet and may be bled using the appropriate syringe.

The pump is shut off, inlet valve (E) closed, bleeder valve (D) closed, and outlet valve (F) opened. The system is now prepared for loading a sample.

2. Sample Loading

When the sample syringe (typically a 250 μl syringe) is removed back pressure from the effluent flask causes a slow leakage of fluid from the end of the sample inlet tube. This prevents air from becoming trapped during changes.

When the sample syringe is loaded, a meniscus is formed so that, when the tubing is connected, the meniscus at the end of the tubing joins it excluding air pockets from the connection.

The medium inlet valve (E in Figure 4.4) is then opened. The medium syringe is disconnected at the inlet valve (E) and filled. Excess air is ejected and a meniscus formed, again preventing air entrapment when the connection is made.

3. Bubble Removal

In most cases, if a bubble is drawn into the system, it collects at the top of the chamber and is readily drawn out using the bleeder syringe.

If a bubble sticks in the electrode chamber, the bleeder syringe is used to force air down to the level of the bubble and the filling procedure (above) used.

4. Flushing

The procedure for flushing is identical to that for sample loading. However clean medium, of the same type as is to be used for the following run, or clean water, if it is a final run of the day, is used for both sample and sheath syringes.

A pump speed of six is usually used as this provides an adequate flush in approximately five minutes.

As every time the sample is loaded there is usually 10 *ml* to 15 *ml* of excess sheath fluid in the medium syringe this, too, is flushed through the system at pump setting six just prior to each run. When the pump plate contacts the sample syringe plunger the pump speed is lowered to fourteen and data logging begins.

APPENDIX D

Sample Preparation

The samples used throughout this work were Polystyrene-divinylbenzene microspheres (8 μm and 5 μm from Duke Scientific) and yeast :

Species:

Saccaromyces cerevesiae

Strain number:

Y1

Source:

the culture collection of the Microbiology Division, Biology Department, University of Calgary

Growth Conditions:

The strain was inoculated to Oxoid (a trade name) Malt Extract Broth. It was grown overnight at 37 C in shaken culture (using a planetary shaker).

The samples were centrifuged and resuspended four to five times in distilled, deionized, and filtered (0.45 μm) water with conductivity adjusted with $K Cl$.

Conductivity measurements were all made using a YSI model 31 conductivity bridge and a YSI 3402 (K=0.1 Ω/cm) probe.

APPENDIX E

A Typical Data Run

1)   Flush system with distilled H_2O.

2)   start up software on HP9816

→   LOAD "DEP_MIN"

→   [Run]

←   Main Menu displayed (see Appendix A)

→   [Time/Date]

←   prompted for time and date

→   [Auto-Run]

←   Auto-Run Menu displayed (See Appendix A)

→   [Init] initialise the IEEE 488 interfaces to all instruments

→   [Printer] commands and data to be logged on printer instead of CRT

→   [Timing]

←   prompt for period in seconds → 35

←   prompt for audible count → N

→   [Select]

← prompt for variable #1 → LOC

prompt for variable #2 → WIDTH

prompt for variable #3 → PK.PK

prompt for variable #4 → [ENTER]

→ [Setup] initialises all equipment to preset status and prints listing of commands issued

3) Prepare sample (See Appendix D)

4) load medium and sample syringes (See Appendix C)

5) set pump speed to six and allow approximately 5 *ml* of medium to flush through the system (no sample is being injected at this time)

6) set pump setting to fourteen

7) set average count on Data 6000 to "0" ([PROC] on the Data 6000 panel)

8) when average count is completed

→ [Prog]

← ?

→ BACK = AVG.A1

← ?

→ .

9) hit [R/S] on the Data 6000 front panel to execute internal program

10) obtain "CONV.A1" on the upper display and "TRLOC" on the lower trace of the Data 6000

11) set the pump speed to six until the push plate of the pump comes in contact with the sample syringe plunger

12) set pump speed to fourteen

13) Run

←   - page ejects

- date and time are printed at the top of the page

- column headings printed for data to follow

14) Wavetek

←   Amplitude?

→   0

- does not prompt for frequency with zero amplitude

- displays "FIELD OFF" on Wavetek display

- prints "FIELD OFF" on printout beside time of execution

15) when the stream appears stable (ie LOC varies less than three or four pixels for three or four readings and PK.PK $>\approx$ 0.025, and the Data 6000 displays a clear peak)

→   Wavetek

←   Amplitude?

→   10 (whatever the user selects)

←   Frequency?

→   10.0E6 (whatever the user selects $50E6 > frequency > 0$)

16) wait for stream to stabilise (approximately 2.5 to 3 minutes)

17) if still sufficient medium go to 13) above, otherwise

18) turn off pump

19) $\boxed{\text{Stop}}$

20) go to 4) above